POLITECNICO DI TORINO

Collegio di Ingegneria Chimica e dei Materiali

Corso di Laurea Magistrale
in Ingegneria Chimica e dei Processi Sostenibili

Tesi di Laurea Magistrale

Gas permeability of composites with cellulosic fillers

Relatori

prof. Bongiovanni Roberta Maria
dott.sa Dalle Vacche Sara
prof. Vanni Marco
firma del relatore (dei relatori)

Candidato

Tran Ngoc Khanh Linh
firma del candidato

Marzo 2021

Il packaging gioca un ruolo importante nell'industria. È presente in numerosi ambiti come cibo e bevande, sanità, cosmetici per garantire la qualità dei prodotti. A causa delle preoccupazioni crescenti per la protezione dell'ambiente, i materiali ottenuti da biomasse come la cellulosa diventano attraenti e vanno a sostituire i materiali sintetici come vetro, alluminio e materie plastiche fossili. I nanocompositi di cellulosa hanno buone proprietà barriera in grado di proteggere i prodotti dall'ambiente esterno, e sono dunque interessanti per applicazioni nel campo degli imballaggi: l'obiettivo di questa tesi è lo studio e la modellazione della loro permeabilità all'ossigeno.

La tesi comprenderà cinque sezioni: introduzione, revisione della letteratura sui compositi con riempitivi cellulosici, permeabilità ai gas in polimeri e compositi, modellazione della permeabilità ai gas e conclusioni. Per condurre la ricerca di letteratura sul tema dei compositi nanocellulosici e sulla loro permeabilità all'ossigeno, i contenuti sono stati accuratamente selezionati e studiati in profondità. Inoltre, è stata realizzata una simulazione sul software ANSYS Fluent sfruttando l'analogia tra il trasporto di calore e la permeabilità attraverso compositi con riempitivi cellulosici. La simulazione si è basata sui dati di Galland *et al.* (2014) e successivamente i risultati sono stati confrontati con altri dati di letteratura.

La cellulosa è il polimero naturale più abbondante sulla terra. E' caratterizzata da basso costo, biocompatibilità, buone proprietà meccaniche ed elevata stabilità chimica. Grazie alle proprietà vantaggiose, la cellulosa è adatta a molte applicazioni come la produzione di carta, l'abbigliamento, i cosmetici, i biomedicali e gli imballaggi. La cellulosa $(C_6H_{10}O_5)_n$ è uno dei polimeri organici più onnipresenti nel pianeta, poiché è una componente pricipale significativa della parete cellulare primaria delle piante verdi. È un polimero polisaccaridico lineare costituito da centinaia a migliaia unità ripetitive di β(1 → 4) legato d-glucose. Le pareti cellulari delle cellule vegetali attribuiscono la loro resistenza meccanica alla cellulosa. La reattività della cellulosa è determinata dalle interazioni molecolari, dalla reticolazione, dalla lunghezza della catena e dai gruppi funzionali.

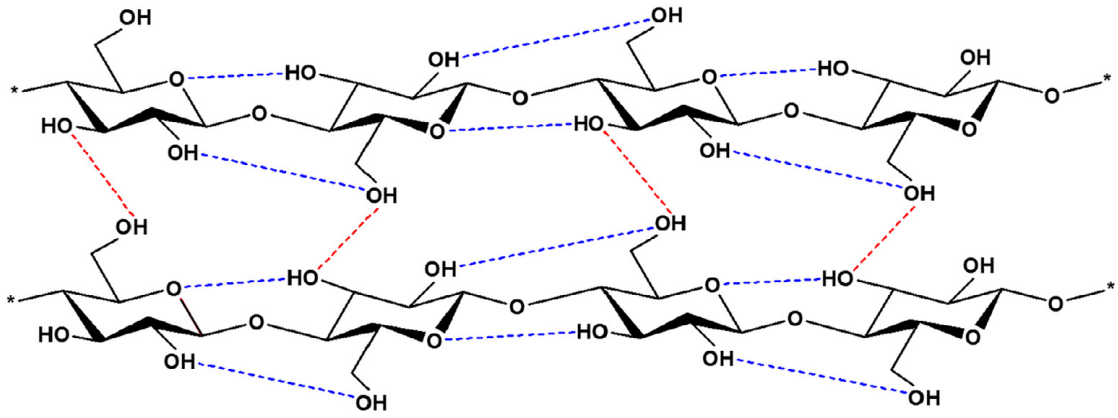

Figura 1 Struttura della cellulosa con reti di legami idrogeno intramolecolari (---) e intermolecolari (---) (Phanthong *et al.*, 2018).

La cellulosa è il componente principale della parete cellulare delle piante, particolarmente le fibre naturali. Le fibre naturali a base di cellulosa sono ottenute da varie parti delle piante. Le fibre di cellulosa naturale possono essere classificate come in Figura 2. Una singola fibra in una pianta contiene più cellule formate principalmente da tre tipi di polimeri: lignina, emicellulosa e cellulosa. La percentuale di lignina, emicellulosa e cellulosa in ciascuna parete cellulare cambia a seconda delle fonti di fibre, come mostrato in Tabella 1.

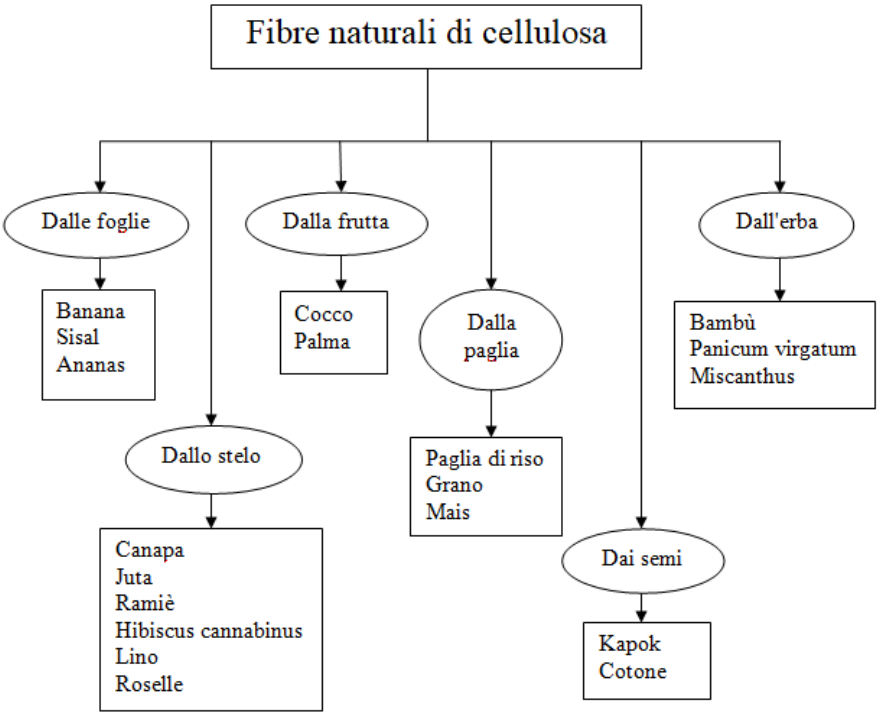

Figura 2 Classificazione delle fibre di cellulosa naturale (Venkatarajan and Athijayamani, 2020).

Tabella 1 Composizione delle diverse fibre naturali (Venkatarajan and Athijayamani, 2020).

Fibre	Cellulosa (wt %)	Emicellulosa (wt %)	Lignina (wt %)	Contenuto di umidità (wt %)
Juta	60.9 – 72.1	14.2 – 20.3	12 – 13	12.7 – 13.6
Lino	71	18.6 – 20.6	2.2	8 – 12
Canapa	70 – 74	17.9 – 22.4	3.7 – 5.7	6.2 – 12
Sisal	66 – 78	10 – 14	10 – 14	10 – 22
Hibiscus cannabinus	45 – 57	21.5	8 – 13	-
Ramiè	68.6 – 76.2	13.1 – 16.7	0.6 – 0.7	7.5 – 17
Banana	63 – 64	10	5	10 – 12
Ananas	70 – 82	-	5 – 12.7	11.8
Cotone	85 – 90	5.7	-	7.85 – 8.5

Le fibre cellulosiche naturali con le caratteristiche di essere a bassa densità, forti, flessibili, relativamente reattive, facili da separare e soprattutto eco-compatibili, sono preferibili in sostituzione delle fibre convenzionali, di vetro, di carbonio, aramidiche. Le fibre cellulosiche naturali sono ampiamente utilizzate come materia prima nell'industria edile, farmaceutica, carta, abbigliamento, cosmetici, imballaggio, alimentare, automobilistico e aeronautico.

Le nanocellulose sono cellulose lavorate in modo da ottenere dimensioni nanometriche. A seconda dei diversi tipi di fonte, struttura, metodi di lavorazione, si possono avere tre tipi di nanocellulose: nanocristalli di cellulosa (CNC), cellulosa nanofibrillata (CNF) e nanocellulosa

batterica (BNC). La Tabella 2 esprime le differenze in termini di dimensioni, origini, metodi, proprietà e applicazioni delle tre categorie di nanocellulosa.

Tabella 2 La famiglia delle nanocellulose

Grado di polimerizzazione	Metodo di produzione e le proprietà		Applicazioni
≥ 500	Delaminazione della pasta di legno mediante pressione meccanica prima e / o dopo il trattamento chimico o enzimatico	Bassa densità, ampia area specifica, buona barriera, proprietà meccaniche e colloidali significative	Parte interna automobilistica, pellicole antiriflesso, substrati per determinare l'attività della cellulasi.
500 – 15,000	Idrolisi acida della cellulosa da molte fonti	Bassa densità, basso coefficiente di espansione termica, elevata resistenza alla trazione, elevata area superficiale, morfologia allungata, facilità di bioconiugazione	Materiale di rinforzo in matrice polimerica, rinforzo in carta, applicazione bio come biosensing, somministrazione di farmaci, impalcatura di ingegneria dei tessuti, applicazione cosmetica, confezionamento alimentare, modificatore di reologia, applicazione di bioimaging, applicazione elettronica.
4000 – 10,000	Sintesi batterica	Nanostruttura unica, purezza, stabilità dimensionale superiore, maggiore resistenza meccanica, maggiore capacità di trattenere l'acqua	Applicazioni biomedicali, impalcatura di ingegneria dei tessuti, pelli artificiali, pellicola trasparente ottica, diaframmi in altoparlanti e cuffie, membrana filtrante nel trattamento dell'acqua, legante nella produzione di carta, proprietà ignifughe in carta sintetica.

Nanocellulosa	Fonti tipiche	Taglia media	
Cellulosa nanofibrillata (NFC)	Legno, barbabietola da zucchero, canapa, lino	Diametro: 5–60 nm	Lunghezza: alcuni micrometri
Nanocristalli di cellulosa (NCC)	Legno, cotone, canapa, lino, paglia di grano, ramiè, avicel, tunicina, cellulosa da alghe e batteri	Diametro: 5–70 nm	Lunghezza: 100–250 nm (da cellulose vegetali); Da 100 nm a alcuni micrometri (da cellulose di tunicati, alghe, batteri)
Nanocellulosa batterica (BNC)	Zuccheri e alcoli a basso peso molecolare	Diametro: 20–100 nm	Lunghezza: >1000 nm

Le nanocellulose sono ampiamente utilizzate nell'industria in applicazioni biomediche, somministrazione di farmaci, imballaggi alimentari e ingegneria dei tessuti. Hanno costo moderato, alto rapporto di aspetto, elevata area superficiale, buone proprietà meccaniche, ottima rigidità, bassa densità. Sono anche considerate come costituenti potenziali di compositi sostenibili, di cui la nanocellulosa può migliorare le proprietà meccaniche e di barriera ai gas, e migliorare la biodegradabilità del composito.

Nanocomposito è un termine usato per un materiale che ha due fasi in cui almeno una delle fasi ha una dimensione nanometrica, nell'intervallo 1-100 nm. Le caratteristiche dei materiali nanocompositi dipendono dalle caratteristiche sia del rinforzo che della matrice, dalla concentrazione e distribuzione delle fasi, dalla forma, le dimensioni e le proporzioni. A causa della struttura in nanoscala, le proprietà meccaniche dei materiali migliorano notevolmente. Alcuni metodi di lavorazione dei nanocompositi a base di cellulosa tra cui estrusione, iniezione, casting / evaporazione, *in situ* polymerization, elettrofilatura vengono impiegati.

Tuttavia, i riempitivi cellulosici, che contengono numerosi gruppi idrossilici, hanno un comportamento idrofilo, trovano difficoltà a connettersi con la superficie idrofobica della matrice polimerica. Per ovviare a questo svantaggio, molti ricercatori e autori hanno studiato e riportato i risultati ottenuti modificando la superficie della cellulosa. La struttura chimica contenente gruppi idrossilici disponibile per le modifiche al fine di migliorare l'interazione superficiale e le proprietà barriera. Si dividono in tre categorie principali: polimeri ad innesto, metodi chimici e adsorbimento.

Le nanocellulose hanno dimensioni nanometriche e una natura cristallina elevata, in grado di formare legami idrogeno costruendo delle reti molto forti che le rendono molto resistenti alle

molecole. L'aggiunta di nanocellulosa nei biopolimeri non solo migliora le proprietà meccaniche come la resistenza alla trazione (circa 104–154 MPa) e il modulo di Young (15,7–17,5 GPa), ma migliora anche le proprietà barriera per i materiali che sono costantemente richiesti per le applicazioni di imballaggio.

Una delle caratteristiche più importanti dei materiali di imballaggio è la prevenzione del contatto tra il prodotto e l'ambiente come la trasmissione di ossigeno e umidità. I polimeri che incorporano nanocellulosa si sono rivelati vantaggiosi nel migliorare la permeabilità all'ossigeno rispetto ai polimeri stessi (Tabella 3).

Tabella 3 Dati di permeabilità all'ossigeno dei nanocompositi

	Nanocellulosa	Polimero		Composito		Permeabilità			
Riferimento	Tipo di nanocellulosa	Nome	Tipo	Metodo di produzione	Cellulosa (vol%)	Permeabilità (cc mm m^{-2} day^{-1} kPa^{-1})	Strumento	Temperatura (°C)	RH (%)
Galland *et al.*, 2014	Cellulosa nanofibrillata (CNF)	Poliestere acrilato iper-ramificato (HBP) CN2302 (Sartomer)	Fotocurabile	-	0	37	Analizzatore di permeazione di ossigeno (Systech 8001)	23	0
				Scambio di solventi + polimerizzazione UV	10	ca 20		23	0
					40	ca 10		23	0
					60	ca 9		23	0
				-	100	0.002		23	0
Martínez-Sanz *et al.*, 2013	Nanocellulosa batterica (BNC)	Il polilattide semicristallino (PLA)	Termoplastica	Tecnica di elettrofilatura	41.7 - 50	17.28	Oxtran 100 attrezzature	24	80
								24	80
		Glicole polietilenico 900 (PEG)			66.7	0.035		24	0
						619		24	80
Jung *et al.*, 2020	Cellulosa nanofibrillata (CNF)	Acido polilattico (PLA)	Termoplastica	-	0	318.38 ± 12.24	analizzatore della velocità di trasmissione dell'ossigeno (Modello: 702, MOCON)	23	0
				Miscelazione	0.21	311.37		23	0
					0.41	222.26		23	0
					0.83	294.7		23	0

Tabella 3 (Cont.) Dati di permeabilità all'ossigeno dei nanocompositi

	Nanocellulosa	Polimero		Composito		Permeabilità			
Riferimento	Tipo di nanocellulosa	Nome	Tipo	Metodo di produzione	Cellulosa (vol%)	Permeabilità (cc mm m^{-2} day^{-1} kPa^{-1})	Strumento	Temperatura (°C)	RH (%)
Djordjevic *et al.*, 2016	Nanocristalli di cellulosa (CNC)	Polietilene (PE) + Policaprolattone (PCL)	Termo plastica	-	0	21.2	Lyssy GPM-200, Gasukuro Kogyo GC-320, HP integrator e 3396.	23	-
				Miscelazione e stratificazione	3.82	3.8		23	-
					7.63	3.2		23	-
					11.45	3.81		23	-
Sanchez-Garcia and Lagaron, 2010	Nanowhiskers di cellulosa (CNW)	Acido polilattico (PLA)	Termo plastica	-	0	1183.7	Oxtran 100 attrezzatura	24	80
				Colata di cloroformio	0.83	198.7		24	80
					1.67	121		24	80
					2.5	129.6		24	80
					4.17	138.24		24	80

I riempitivi nanocellulosici sono particolarmente interessanti se utilizzati in combinazione con polimeri biobased poiché sia il riempitivo che la matrice si comportano in modo rispettoso dell'ambiente. Si osserva che l'acido polilattico (PLA) è un polimero attraente quando viene utilizzato come matrice rinforzata per il riempitivo di nanocellulosa. Inoltre, si osserva che la permeabilità all'ossigeno dei nanocompositi diminuisce all'aumentare della frazione volumetrica dei filler cellulosici.

Dopo uno stato dell'arte, il lavoro di tesi ha incluso l'uso di un modello di simulazione utilizzando il software ANSYS Fluent per prevedere la riduzione della permeabilità dei compositi quando vengono aggiunti riempitivi cellulosici. La simulazione si è basata sulla soluzione dell'equazione del trasferimento di calore ($\dot{Q}$) per prevedere il trasferimento di massa (J). Il calore viene trasferito in una cella in cui viene applicata una differenza di temperatura tra i due lati, corrispondente a un gradiente di concentrazione del gas. Le particelle vengono aggiunte nella cella per modellare il riempitivo. Vengono testate frazioni di volume del 10%, 40% e 60% delle particelle.

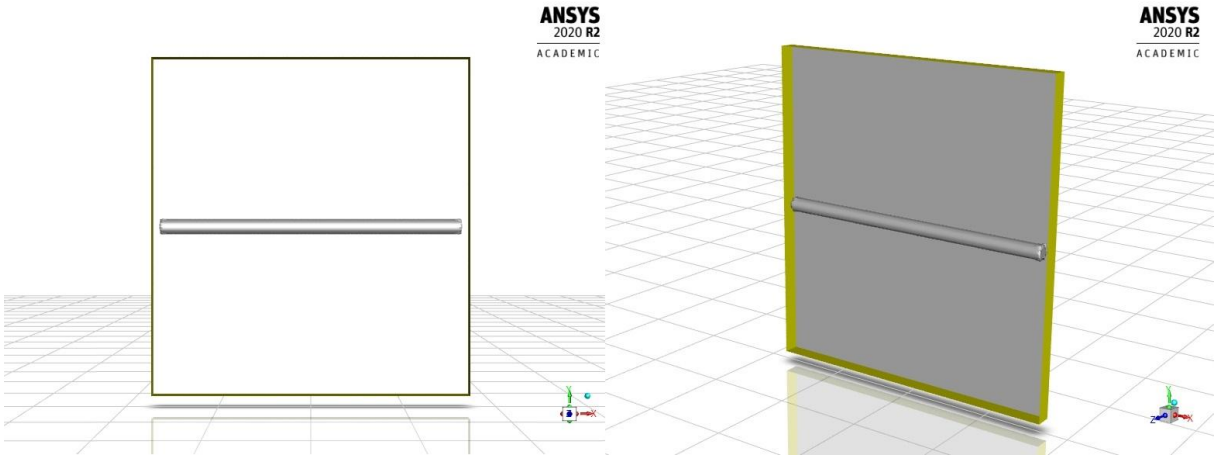

Figura 3 Geometria della cella con una particella

Viene calcolato il rapporto R del flusso di calore con e senza particelle

$$R = \frac{\dot{Q}_{\text{con particelle di cellulosa}}}{\dot{Q}_{\text{senza particelle di cellulosa}}}$$

Dove $\dot{Q}$ con particelle di cellulosa viene acquisito dalla simulazione su ANSYS Fluent.

$$\dot{Q}_{\text{senza particelle di cellulosa}} = k\frac{\Delta T}{\delta}A$$

Quindi anche:

$$R = \frac{J_{\text{con particelle di cellulosa}}}{J_{\text{senza particelle di cellulosa}}}$$

Dalla simulazione, $\dot{Q}$ diminuisce con l'aumento della frazione volumetrica delle particelle: $\dot{Q}$ (nessuna particella) > $\dot{Q}$ (10 vol% di particelle) > $\dot{Q}$ (40 vol% di particelle) > $\dot{Q}$ (60 vol% di particelle). Allo stesso modo la permeabilità all'ossigeno diminuisce all'aumentare della

frazione volumetrica delle cariche cellulosiche. Il risultato conferma precedenti ricerche di Galland et al. (2014), Jung *et al.* (2020), Djordjevic *et al.* (2016), Sanchez-Garcia e Lagaron (2010). È stato osservato anche che le posizioni e il rapporto di aspetto delle particelle influenzano la permeabilità. I risultati della simulazione sono considerati come un esercizio preliminare in cui possono essere condotti miglioramenti al fine di ottenere i risultati più ravvicinati come esperimenti reali. Gli effetti della temperatura, del livello di umidità e della complessità nella forma delle cariche cellulosiche non sono considerati nella simulazione, e possono essere oggetto di ricerche successive.

Indice

1. Introduction

Packaging holds a vital role in our everyday life. Methods of packaging are presented in various industries to guarantee the quality and preserve the products, such as food and beverage, health care and cosmetics. Due to increasing concerns regarding the environment impact of plastic packaging, materials made from bio resources like cellulose are gradually replacing synthetic materials such as glass, aluminum, and fossil-fuel plastics. Cellulose nanocomposites have been found to have excellent barrier properties, which could be utilized to preserve the packaged products and prevent the effect of external environment.

Cellulose is the most abundant natural polymer on earth, with the characteristics of low cost, biocompatibility, tailored mechanical properties and high chemical stability. With these advantageous properties, cellulose found applications in many industries: wood, paper production, clothes, cosmetics, biomedical and packaging. One major application of cellulose is through the form of nanocellulose. Nanocelluloses are processed cellulose in nano size. There are three types of nanocellulose: Cellulose nanocrystals (CNCs), cellulose nanofibrils (CNFs) and bacterial nanocelluloses (BNCs). Nanocelluloses have the properties of low cost, high aspect ratio, high surface area, improved mechanical properties and excellent stiffness. Nanocelluloses are widely used in biomedical applications, drug delivery, food packaging and tissue engineering. They are also considered as potential constituent in composite sustainable processes.

This research expands on the topic of nanocellulose composites as well as their oxygen permeability, drawing from literatures and thoroughly studying them in depth. A simulation was built on ANSYS software to observe the permeability through cellulosic fillers based on the analogy between heat and permeability. The simulation based on the research and scenario in Galland *et al.* (2014), afterward the results are compared with different scenarios in literature.

The thesis will encompass five sections: introduction, literature review on composites with cellulosic fillers, literature review on gas permeability in polymers and composites, modelling gas permeability and conclusion.

Chapter 2 will include review of literature focusing on the concept of cellulosic fillers including natural fibers, cellulose nanocrystals (CNCs), cellulose nanofibrils (CNFs) and bacterial nanocelluloses (BNCs). Resources, outstanding characteristics, processing methods and applications for each type of cellulose are introduced. In chapter 3, the thesis will discuss oxygen permeability of materials. Definitions and different standard methods for measuring oxygen transmission rate are explained. Data collection of oxygen permeability of polymers and composites with cellulosic fillers are provided. In chapter 4, the thesis aims to build a simulation using ANSYS software for observing the reduction of oxygen permeability of composites when cellulosic fillers are added. Due to the analogy between heat and mass transfer, the simulation observed change in heat transfer when adding cellulosic fillers to predict change in permeability. It was observed that the oxygen permeability decreased when volume fraction of cellulosic fillers increased.

2. Composites with cellulosic fillers

With the development of novel technology and rising concerns toward environmental issues, materials that are non-toxic, biocompatible, renewable, with low cost and low energy consumption are becoming more favorable in manufacturing industry. As such, natural fibers, especially cellulosic fibers have garnered growing interest from researchers and scientists. Cellulose is a compound existing in abundant volume from inexhaustible sources in nature; it is a biopolymer that comes from natural fibers in plants, vegetables, and some organisms, with annual production of approximate 75-100 billion tons (Sankhla *et al.*, 2020).

2.1 Cellulose

Cellulose is a linear polysaccharide polymer composed of several hundred to thousands repeating cellobiose units, containing β-1,4-linked anhydro-D-glucose units as showed in Figure 2.1.1.

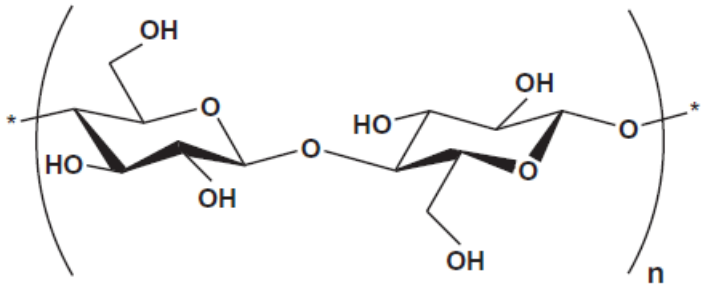

Figure 2.1.1 Structure of cellobiose (Phanthong *et al.*, 2018)

The reactivity of cellulose is driven by molecular interactions, cross-linking, chain length and by the functional groups (Klemm *et al.*, 2005). The covalent bonds in pyranose ring and between every cellulose unit make cellulose very resistant to tensile stress. Cellulose is known to have hydrogen bonds which are intramolecular and intermolecular (Hinterstoisser *et al.*, 2003). Figure 2.1.2 shows the structure of cellulose with these two types of hydrogen bonding (Phanthong *et al.*, 2018). With this unique structure, cellulose has excellent mechanical and physical properties, which enables cellulose as an ideal material for barrier applications (Syverud and Stenius, 2008).

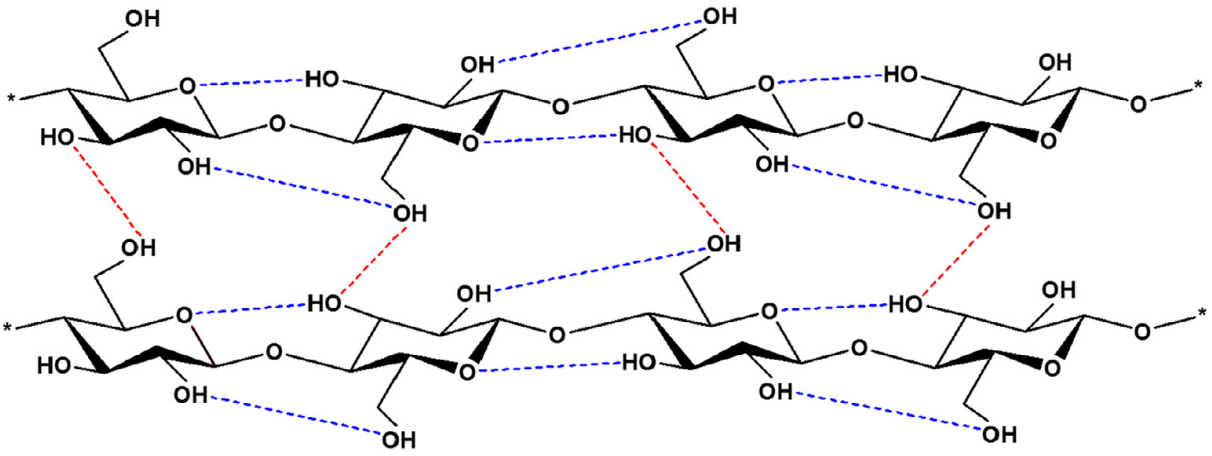

Figure 2.1.2 Cellulose structure with intramolecular (---) and intermolecular (---) hydrogen bonding networks (Phanthong *et al.,* 2018).

Generally, there are four different crystalline polymorphs of cellulose, namely cellulose I, II, III, IV. Cellulose I is native cellulose, which is the main component in plants. Cellulose I has two different structures: cellulose Iα found mainly in microbes, and cellulose Iβ which is extracted from cell wall of plants (Xu and Wang, 2015). Cellulose II is obtained by chemical regeneration by dissolving cellulose I in a solvent or swelling cellulose I in acid or alkaline solution. Cellulose II is the most thermodynamically stable among all four polymorphs of cellulose (Lavanya *et al.*, 2011; Habibi *et al.*, 2010). On the other hand, polymorph cellulose III_I and III_{II} are acquired by the treatment of cellulose I and II in gas or liquefied ammonia or in series of amines. Heating cellulose III at 260^{o}C with glycerol will produce cellulose IV (Wada *et al.*, 2001).

2.2 Cellulosic fillers

2.2.1 Cellulosic fibers

Natural fibers are acquired from the three main origins: from plant such as cotton, jute, ramie, hemp, from animal including wool and silk and from mineral including the asbestos group (Sydow and Bieńczak, 2019). Fibers made from plants are called cellulosic fibers or lignocellulosic fibers. A single fiber in a plant naturally contains multiple cells formed by mainly three kinds of polymers: lignin, hemicellulose, and cellulose. The composition of lignin, hemicellulose, and cellulose in each cell wall varies depending on the fiber sources. Cellulose is the main component in plant cell wall. Lignin is an amorphous binder which has both aliphatic and aromatic structures, adheres around cellulose and hemicelluloses. Hemicellulose is a heteropolymer consisting of polysaccharides, which links to cellulose fibrils through hydrogen bonds and Van der Waal's interactions (Bledzki and Gassan, 1998; Phanthong *et al.*, 2018).

Based on sources, natural cellulosic fibers are categorized into different groups. Each group has distinctive properties. Lavanya *et al.* (2011) showed the percentage content of cellulose in each source, reported in Table 2.2.1.1.

Table 2.2.1.1 Cellulose resources

Resources	Examples	% of cellulose
Leaves	Sisal, agave, fique	33
Bast and skin	Flax, jute, hemp, ramie, rattan, vine fibers	61-76
Seeds	Cotton, kapok	90
Fruits	Coconut fiber	30-50
Stalk fibers	Rice, barley, wheat straws, bamboo, grass, tree wood	40-50

The most typical fiber sources are (Textile School, 2019):

- Bast and skin: Including ramie, hemp, jute.
  - Ramie is the oldest fiber crops. They are good absorbent, quick-drying, slightly stiff and naturally lustrous.
  - Hemp fibers are extracted from the stem, possessing an excellent durability, strength, resistance to ultraviolet light and mold, and high absorbency.
  - Jute is the cheapest natural fibers and has the second largest production amount after cotton. It is a lignocellulosic fiber which composed of textile and wood. It is long, soft and has a good resistance to microorganisms and insects.
- Fruit fibers, typically coconut fibers which are extracted from dry mature coconut husk after soaking. They are strong fibers with lower water absorption capacity.
- Seed fibers, typically cotton fibers. Cotton fibers are soft and strong, and can hold water up to 24 – 27 times their own weight. Cotton fibers can stand up against abrasion and high temperature. Another type of seed fiber is kapok fibers. They are silky fibers like cotton, found surrounding the seeds in the pods of ceiba trees. Kapok fibers are eight times lighter than cotton. Kapok fibers have excellent thermal-isolation and good impermeability. They are also non-toxic and resistant to rot. Because of the high degree of fragility, kapok fibers cannot be spun.

Natural cellulosic fibers, with the characteristics of being low-density, strong, flexible, relatively reactive, easy to separate and especially eco-friendly, are preferable to the conventional fibers such as glass, carbon, aramid fibers (Nair *et al.*, 2010). Natural cellulosic fibers are widely used as an energy source (Reese *et al.*, 2005) and raw material in construction, pharmaceuticals, paper, clothing, cosmetics, packaging, food, automotive and aircrafts industries (Sanjay *et al.*, 2016).

Natural cellulosic fibers have a heterogeneous microstructure while synthetic fibers have a homogeneous microstructure. Due to the heterogeneous microstructure, properties of natural fibers would vary in different source characteristics: positions of plant (stems or leaves), age of plant and quality of the location. Instead, synthetic fibers are produced with precise properties. Some examples are shown by a scanning electron microscope (SEM) of synthetic fibers in Figure 2.2.1.1 and of natural fibers in Figure 2.2.1.2.

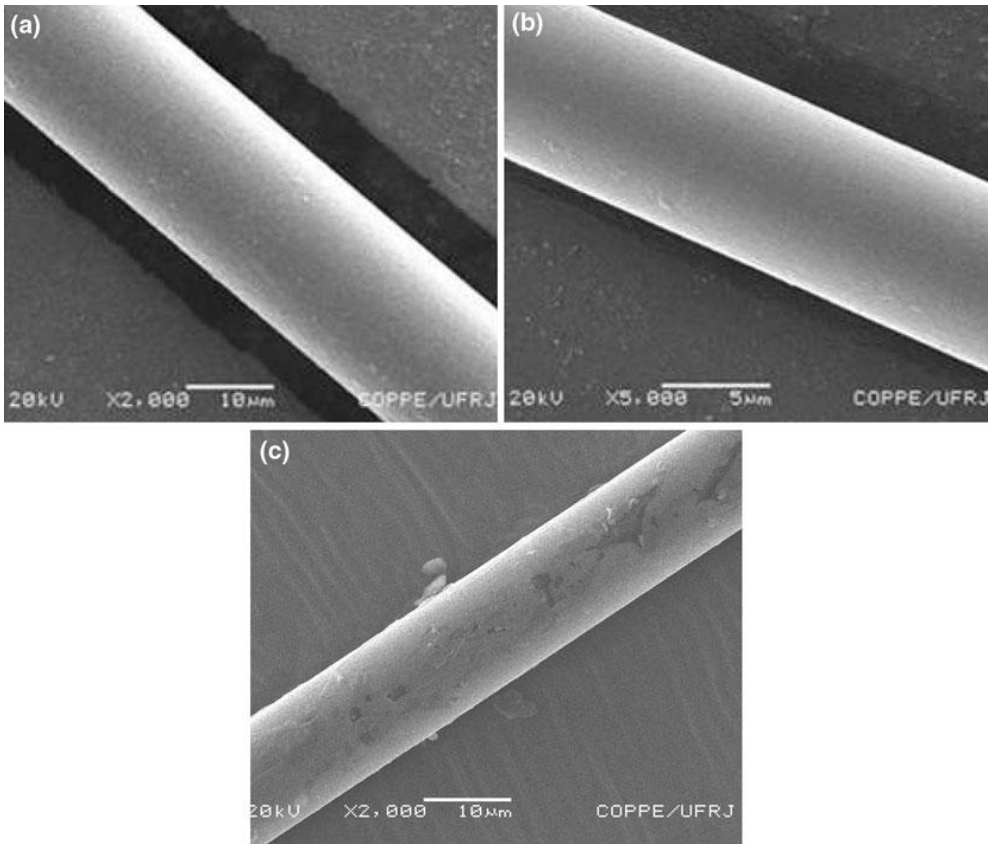

Figure 2.2.1.1 SEM image of conventional fibers: (a) glass, (b) carbon, (c) aramid (Monteiro *et al.*, 2011)

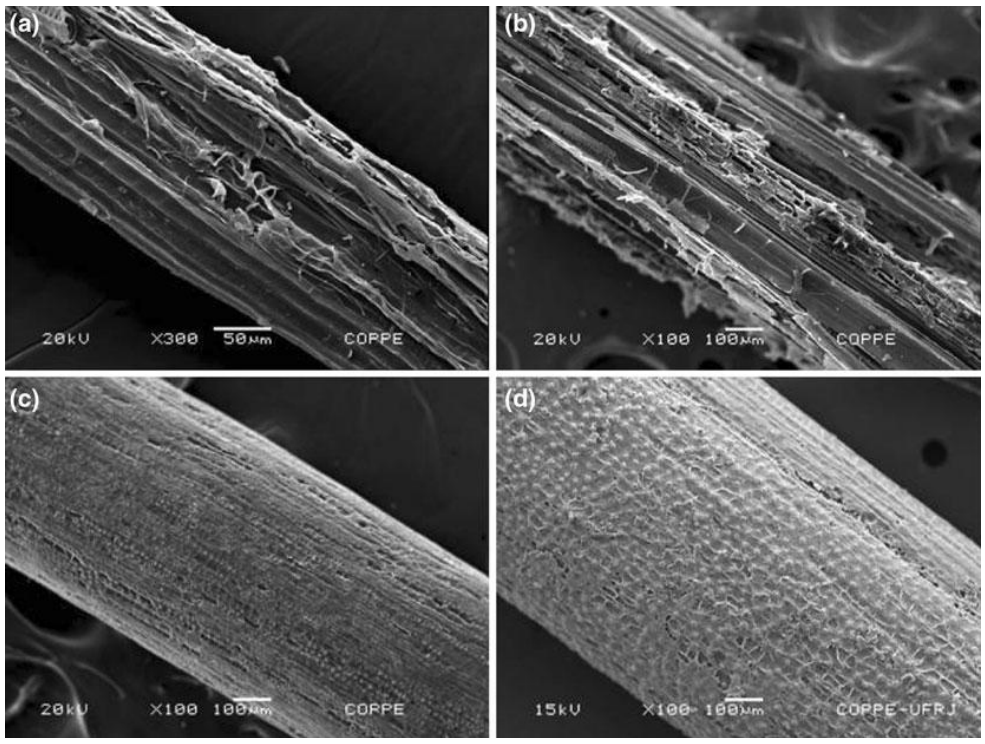

Figure 2.2.1.2 SEM image of natural lignocellulosic fibers: (a) sisal, (b) bamboo, (c) coir, and (d) piassava (Monteiro *et al.*, 2011)

2.2.2 Nanocellulose

Nanocellulose is cellulose processed to nano-sized structure; nanocellulose is combined from two terms: “cellulose” and “nanostructure” (Morán *et al.*, 2008). Nanocelluloses are materials that have dimensions between cellulose molecules and pulp fibers. Despite their discovery long time ago, nanocelluloses’ superior aspects have just been exploited recently. Nanocelluloses are now considered one of the most promising and preferable green materials: the number of scientific research articles related to nanocellulose increases every year, accompanying rapid development of nanotechnology and ecotechnology. Per reports by Markets and Markets (2020), nanocellulose markets are expected to increase from USD 297 million in 2020 to USD 783 million by 2025, further emphasizing the importance and feasibility of nanocellulose’s novel applications (Coelho *et al.*, 2018).

Due to the nano-size dimension, nanocelluloses have excellent mechanical properties, high Young’s modulus, high surface area, high aspects ratios, tunable self-assembly and low density. In their structure, nanocelluloses include both crystalline and amorphous regions. In the crystalline regions, cellulose molecules are arranged in highly structured chains, demonstrating the strength and stiffness of cellulose. On the other hand, the amorphous regions increase the flexibility of nanocellulose (Moon *et al.*, 2016; Phanthong *et al.*, 2018). With these unique properties, nanocellulose is employed in advanced applications including paper products, antibacterial films, reinforced polymer composites, drug delivery and environmental remediation. Especially, nanocellulose is a vital component in the manufacture of nanocomposites and materials based on polymers, metals, carbon, where nanocellulose can consolidate strength and impart biocompatible properties to the composite (Thomas *et al.*, 2018).

Depending on different types of source, structure, maturity, and processing methods, nanocellulose can be obtained in different forms (Klemm *et al.*, 2011; Trache *et al.*, 2020). Mainly, nanocellulose are divided into three groups: (1) Cellulose nanocrystals (CNCs), also known as cellulose (nano) whiskers, nanocrystalline cellulose, (2) cellulose nanofibrils (CNFs) or nano-fibrillated celluloses (NFCs), micro-fibrillated celluloses (MFCs) and (3) bacterial nanocelluloses (BNCs) as microbial cellulose (Lin and Dufresne, 2014).

Cellulose nanocrystals (CNCs) have elongated and short rod-like shape with highly crystalline structure, around 2-20 nm in diameter, 100-500 nm in length. CNCs can be obtained by the process of acid hydrolysis, using sulfuric acid or hydrochloric acid where the amorphous regions are hydrolyzed and removed from cellulose while retaining crystalline regions. CNCs have high crystallinity index around 54-88%. (Phanthong *et al.*, 2018; Mu *et al.*, 2019; Trache *et al.*, 2020).

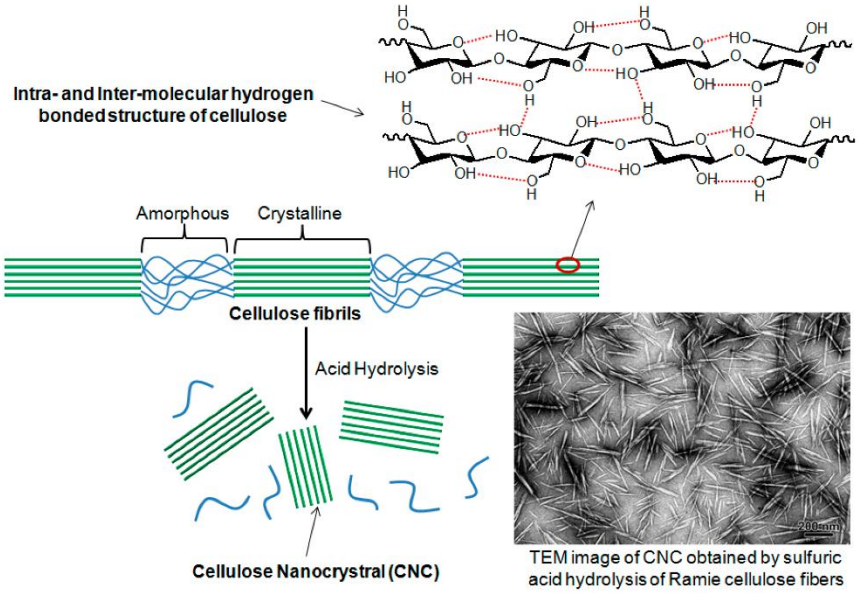

Figure 2.2.2.1 Production of cellulose nanocrystals (CNC) (Chakrabarty and Teramoto, 2018)

Cellulose nanofibrils (CNFs), also called nano-fibrillated cellulose which are made from fibers chain chemically composed of 100% cellulose, including both crystalline and amorphous regions. CNF are long fibrils with length greater than 10,000 nm. CNF are acquired using a process of mechanical, chemical, and biological methods, where mechanical approaches primarily include homogenizers, grinders and microfluidizers. Chemical and enzymatic pretreatments are employed to reduce the energy consumption of mechanical fibrillation which is reported around 4500–10000 kWh/ton (Nair *et al.*, 2014). Compared to CNC, they are longer, have high aspect ratio, high surface area but lower crystallinity (Phanthong *et al.*, 2018; Naz *et al.*, 2019).

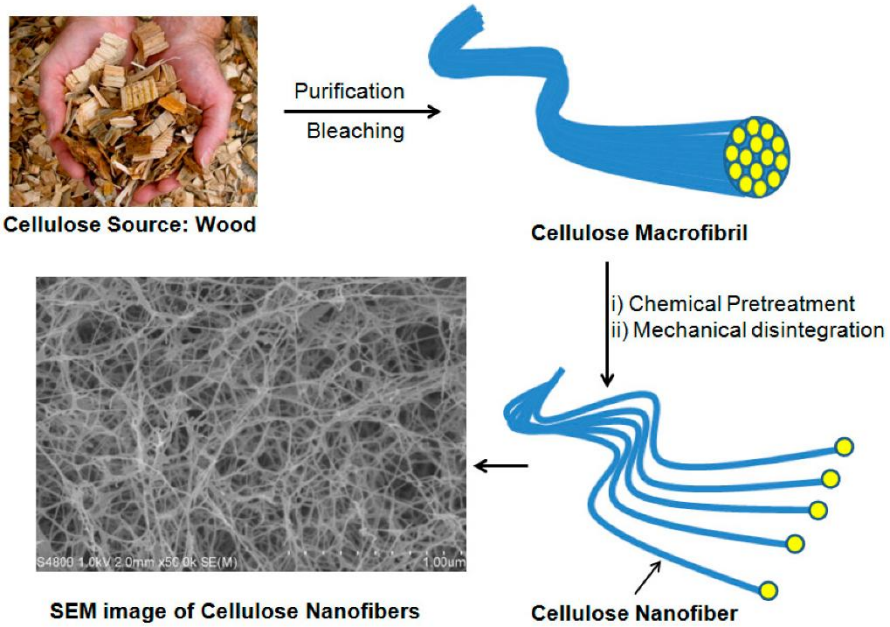

Figure 2.2.2.2 Production of cellulose nanofibrils (CNF) (Chakrabarty and Teramoto, 2018)

Differently from CNC and CNF, bacterial nanocelluloses (BNC) are not extracted from plant. They are grown up biosynthetically from sugar molecules using bacteria Gluconacetobacter xylinus cultivated in a growth medium such as rotten fruits or milk whey, mainly from industrial waste (Jozala *et al.*, 2014). Bacterial cellulose molecules are produced inside bacteria and are then extracted through the pores of the outer membrane of the bacterial cell (Liu *et al.*, 2020). BNC has a three-dimensional network consisting of ultrafine ribbon-shaped nanofibers with diameter of 20-100 nm and length of several micrometers. BNC is insoluble in water, durable and elastic. In addition, BNC is composed purely of cellulose without lignin, hemicelluloses or other compound; therefore, the purification of bacterial cellulose is easier, cheaper, and more biocompatible compared to nanocelluloses extracted from plants. In term of size, BNC is smaller than CNC and CNF and has better mechanical properties (Jozala *et al.*, 2016; Lin *et al.*, 2020).

Table 2.2.2.1 summarizes studies from Klemm *et al.* (2011), Klemm *et al.* (2018), Trache (2018) and Rashid *et al.* (2018), showing the differences in size, origins, methods, properties and applications of the three main families of nanocellulose.

Table 2.2.2.1 The family of Nanocellulose

Terminology and nomenclature of nanocellulose	Typical sources	Average size	Degree of polymerization	Production method and properties	Applications
Nano- or microfibrillated cellulose (NFC/MFC), cellulose nanofibril, nanofibrillar cellulose	Wood, sugar beet, potato tuber, hemp, flax	Diameter: 5–60 nm	≥ 500	Delamination of wood pulp by mechanical pressure before and/or after chemical or enzymatic treatment	Interior automotive part, antireflective films, substrates to determine cellulase activity.
		Length: several micrometers		Low density, large specific area, good barrier, significant mechanical and colloidal properties	
Nanocrystalline cellulose (NCC), cellulose nanocrystals, crystallites, whiskers, rodlike cellulose, microcrystals	Wood, cotton, hemp, flax, wheat straw, mulberry bark, ramie, Avicel, tunicin, cellulose from algae and bacteria	Diameter: 5–70 nm	500 – 15,000	Acid hydrolysis of cellulose from many sources	Reinforcing material in polymeric matrix, paper reinforcement, bio application like biosensing, drug delivery, tissue engineering scaffold, cosmetic application, food packaging, rheology modifier, bioimaging application, electronic application.
		Length: 100–250 nm (from plant celluloses); 100 nm to several micrometers (from celluloses of tunicates, algae, bacteria)		Low density, low coefficient of thermal expansion, high tensile strength, high surface area, elongated morphology, ease of bioconjugation	
Bacterial nanocellulose (BNC), microbial nanocellulose, biocellulose	Low-molecular weight sugars and alcohols	Diameter: 20–100 nm	4000 – 10,000	Bacterial synthesis	Biomedical applications, tissue engineering scaffold, artificial skins, optical transparent film, diaphragms in speakers and headsets, filtration membrane in water treatment, binder in paper production, fire-retarding properties in synthetic paper.
		Length: >1000 nm		Unique nanostructure, purity, higher-dimensional stability, greater mechanical strength, greater capacity to hold water	

2.3 Composites

2.3.1 Composites with natural cellulosic fibers

Polymers are playing an important role in the entire world and exist in almost every aspect of life, from daily necessities, biomedical to defense fields. Polymer based composite materials have found widespread industrial usage: such as automotive, aerospace, electronic devices, furniture, construction etc. Composites are materials consisting of two or more distinct constituents, matrix and reinforcement that exist separately and have different properties. One major usage of natural cellulosic fibers is the materials of reinforced polymer composites. In polymer composites, the fibers play as the reinforcement which is the main component controlling the properties of the material. Polymers are the matrix which carries loads along the reinforcement (Thakur and Thakur, 2014; Thyavihalli Girijappa *et al.*, 2019).

Polymer composites are divided into several categories depending on the nature and type of reinforcement and polymer. Based on the characteristics of the reinforcement, polymer composites are classified into fibers reinforced polymer composites and particles reinforced polymer composites. In fibers reinforced polymer composites, the reinforcement is in the form of fibers, from either synthetic or natural fibers. On the other hand, in particles reinforced polymer composites, the reinforcement is produced in form of particles with various dimensions. Another method of categorizing polymer composite is based on the effect of the composite on the environment. Polymer composites are divided into 100% renewable composites, where both reinforcement and the matrix came from renewable resources; partly renewable composites, where either reinforcement or the matrix is renewable; and nonrenewable composites, where none of the composites' components are renewable resources (Thakur and Thakur, 2014).

Natural cellulosic fiber composites are preferable over synthetic fibers such as glass and carbon fibers due to their low cost, low density, renewability, and biodegradability leading to less environmental damage. However, besides these advantages there are some limitations on natural cellulosic fiber composites when compared to synthetic fibers. They have numerous hydroxyl groups inducing hydrophilic behaviors, which have poor compatibility with hydrophobic property of polymer matrix, resulting in reduced the impact strength and mechanical properties. The hydrophilicity tends to absorb moisture causing poor moisture resistance of materials. Moreover, the moisture absorption of natural fibers affects their thermal stability as well. The high level of moisture leads to micro-cracking and low thermal stability degrades the composite (Venkatarajan and Athijayamani, 2020; Azwa *et al.*, 2012).

The component that affects the moisture absorption of natural fibers is hemicelluloses which are the most hydrophilic. Increase in hemicelluloses content would result in higher moisture absorption of fibers. Surface modifications such as chemical treatments are necessary in order to lower the moisture absorption. Alkaline treatment is applied by using potassium hydroxide (KOH) or sodium hydroxide (NaOH) to remove the open hydroxyl groups responsible for bonding with water. In addition, the hydroxide dissolves hemicelluloses, reducing moisture absorption capacity (Thyavihalli Girijappa *et al.*, 2019; Azwa *et al.*, 2012).

Silane treatment is another process helping stabilizing interfacial connection between natural fibers and polymers as well as avoiding moisture penetration. Silane is added in cavities on the outer layers of fibers hiding vacancies for water to entering. However, this treatment is

less effective due to its temporary function that still allow water penetrate with low rate, since silane polymers do not fully block the cell walls (Azwa *et al.*, 2012).

Acetylation introduces an acetyl group to the surface of fibers. Acetyl groups react with hydroxyl groups on fibers making the fibers more hydrophobic which are compatible with polymer matrix improving the adhesion between them (Thyavihalli Girijappa *et al.*, 2019).

The mechanical properties of natural cellulosic fiber polymer composites are affected by many aspects: the nature of materials, volume or weight fraction of fibers, their aspect ratio, geometries and orientation, adhesion between fibers and polymers, essential additives and modifications. Higher fiber content in material results in more flexural stress and the higher aspect ratio of the fibers improves mechanical performance of composites (Venkatarajan and Athijayamani, 2020; Thyavihalli Girijappa *et al.*, 2019).

Applications using natural cellulosic fiber polymer composites are growing fast in engineering industry. Natural cellulosic fibers such as jute, hemp, bamboo reinforced polymer composites are attractive in automotive, building materials and construction. They are also found in aerospace, sports, ceilings, office devices and indoor products which are not affected by the environment (Mohammed *et al.*, 2015). Table 2.3.1.1 shows some examples on applications of natural cellulosic fiber composites in industry.

Table 2.3.1.1 Natural cellulosic fiber composites applications (Mohammed *et al.*, 2015)

Fiber	Applications
Hemp fiber	Construction products, textiles, cordage, geotextiles, paper & packaging, furniture, electrical, manufacture bank notes, and manufacture of pipes.
Oil palm fiber	Building materials such as windows, door frames, structural insulated panel building systems, siding, fencing, roofing, decking, and other building materials.
Wood fiber	Window frame, panels, door shutters, decking, railing systems, and fencing.
Flax fiber	Window frame, panels, decking, railing systems, fencing, tennis racket, bicycle frame, fork, seat post, snowboarding, laptop cases.
Rice husk fiber	Building materials such as building panels, bricks, window frame, panels, decking, railing systems, fencing.
Bagasse fiber	Window frame, panels, decking, railing systems, fencing.
Sisal fiber	In construction industry such as panels, doors, shutting plate, and roofing sheets, manufacturing of paper, pulp.
Stalk fiber	Building panel, furniture panels, bricks, and constructing drains and pipelines.
Kenaf fiber	Packing material, mobile cases, bags, insulations, clothing-grade cloth, soilless potting mixes, animal bedding, and material that absorbs oil and liquids.
Cotton fiber	Furniture industry, textile and yarn, goods, cordage.
Coir fibers	Building panels, flush door shutters, roofing sheets, storage tank, packing material, helmets and postboxes, mirror casing, paper weights, projector cover, voltage stabilizer cover, a filling material for the seat upholstery,

	brushes and brooms, ropes and yarns for nets, bags, and mats, as well as padding for mattresses, seat cushions.
Ramie fiber	Products as industrial sewing thread, packing materials, fishing nets, and filter cloths. It is also made into fabrics for household furnishings (upholstery, canvas) and clothing, paper manufacture.
Jute fiber	Building panels, roofing sheets, door frames, door shutters, transport, packaging, geotextiles, and chip boards.

2.3.2 Composites with nanocellulose

Apart from the common applications of cellulose such as paper and textile industry, nanocelluloses are applied as polymer composite reinforcement in the manufacture of a large range of nanocomposite materials.

Nanocomposite is a term used for a material that has two phases in which one of the phases has at least one nanometer dimension, in the range between 1-100 nm (Oksman *et al.*, 2006). The characteristics of nanocomposite materials depend on the characteristics of both the reinforcement and the matrix, such as the concentration and distribution of phases, shape, size and aspect ratio as well. Due to the nanoscale structure, mechanical properties of materials are significantly improved (Raza *et al.*, 2019). Nanocelluloses are combined with polymers in order to improve the properties of polymers while filling the disadvantages of other nanofillers such as carbon nanotube which are expensive, not biodegradable and hard to recycle (Zhu *et al.*, 2017; Feldman, 2015).

Nanocellulose incorporated in polymer matrices mitigates environmental concerns and improves the polymer's biodegradability. Biodegradability is the capacity of materials to be degraded naturally in the environment; i.e. losing their mechanical and structural properties, changing the chemical structure and converting to other compounds which are compatible to the environment (Rashid et al., 2018). Besides the biodegrability, nanocelluloses have high abundance, low specific weight, low filler load requirements, nanoscale structure and high aspect ratio enhancing the impact strength, structural, mechanical and barrier properties which are excellent for developing the polymer nanocomposites manufacture (Pandey *et al.*, 2012).

Compared to CNC, CNF are easier to produce and have a higher yield. Furthermore, CNF are longer and more flexible than CNC, while having greater strength and higher aspect ratio. CNF is a stronger reinforcement in polymers matrix; the amorphous structure of CNF improves flexibility of the material while the crystalline structure represents the stiffness and strength of the material (Zhu *et al.*, 2017; Chaker *et al.*, 2013).

Cellulosic materials tend to agglomerate when they are in dry condition. This happens due to the hydroxyl groups on cellulose surface. It is estimated that the attractive energy of hydrogen bonds in nanocellulose between two CNCs parallel is 7.5×10^{-16} J. This energy is two orders of magnitude higher than van der Waals energy bonds (Kargarzadeh *et al.*, 2017). When CNC particles are immersed in water, the distance between them is calculated of 1.2-1.6 nm which is equal to 4-6 layers of water molecules. Similar results are obtained with some other solvents. Therefore, by swelling cellulose nanocrystals in a suitable solvent, the interaction between CNC can be replaced with the interaction between CNC and the solvent making the film stable (Kargarzadeh *et al.*, 2017). In order to maintain particles immersed in solvent, the simplest approach is mixing directly cellulose nanomaterial and polymer matrix in the same solvent where polymer is soluble in solvent (Dufresne, 2018). On the other hand, the solvent

exchange is introduced to replace water with another proper organic solvent (Kargarzadeh *et al.*, 2017).

Materials using nanocellulose reinforced in organic polymers are commonly used in industry. They are biocompatible that being preferred to apply in many areas such as biomedical, bioplastics, food packaging, coatings and so on. The structure composed of hydrogen bonding enhances the strength and stiffness of the materials, which enables excellent mechanical properties while improving thermal and optical properties of the composite materials (Thomas *et al.*, 2018). Thermoset polymers such as polyurethane (PU) and epoxy and thermoplastic polymers like polylactic acid (PLA), polyethylene (PE), polypropylene (PP), poly(propylene carbonate) (PPC), poly(vinyl alcohol) (PVA) and poly(ethylene oxide) (PEO) are all utilized as organic reinforced matrix (Lu *et al.*, 2014).

Table 2.3.2.1 Examples of techniques applied in cellulose nanocomposites processing (Kargarzadeh *et al.*, 2017; Martínez-Sanz *et al.*, 2013; Hatch *et al.*, 2019)

Process	Polymer matrix	Cellulose source	Fraction (wt%)
Extrusion	PLA	Ramie	0-3
	PE	Ramie	0-15
	PEO	Cotton	0-9
	PS	Cotton	0-20
	PVAc	Paper	0-12
Injection	PA-6	Cotton	0-1
	PHBV	MCC	2-5
Casting/evaporation	Epoxy resin	Cotton	0-24
	Natural rubber	Cassava	0-10
	PA-6	MCC	5
	PVA	MCC/Flax	0-5
	PLA	Wood pulp	0-3
		MCC	1-9 phr
In situ polymerization	NR/PS	Bacterial	1-10
	PHBV	MCC	0-10
	PCL	Ramie	0-40
	PNVCL	MCC	0-20
Electrospinning	PLA/PEG	BCN	50-60/80
	PVP	CNC	1-8

Many methods are applied to prepare composites including melt processing, casting and evaporation, in situ polymerization and lamination (Kargarzadeh *et al.*, 2017).

Melt processing including injection molding and extrusion use heat to soften and mold polymers. These methods are applied widely in industry due to the high rate and reproducibility of polymer materials (Kargarzadeh *et al.*, 2017). Casting and evaporation method require suspension of nanocellulose and polymer matrix prepared, the final film products are collected with the highest mechanical properties and the well controlled thickness after removal of solvent by evaporating. However, these methods are limited in laboratory scale due to large amount of solvent required in industrial scale (Kargarzadeh *et al.*, 2017). In *in situ* polymerization method monomer is present with nanocellulose and the polymerization takes place in order to well mix nanofiller in the matrix (Kargarzadeh *et al.*, 2017). The method finds limitations in industry due to the solvent requirement as well. Electrospinning is another method to produce nanocomposites which is widely used in manufacture (Joseph *et al.*, 2020).

Ensuring surface compatibility between reinforcing filler and continuous matrix material is the most important and significant step in nanocellulose composite processing, including the dispersion of the filler in the polymer matrix and the surface adhesion between the two materials. Each type of nanocellulose relies on particular production mechanism that influences behaviors of the surface of reinforcing filler when reacting with matrix material, considered as the prerequisite for composite proceeding classifies different methods and characteristics of the reinforcement.

Cellulosic fillers, which contain numerous hydroxyl groups with hydrophilic behavior, find difficulty in connecting with the hydrophobic surface of polymer matrix material. Therefore, over the years, many researchers and authors have studied and reported the achievements by modifying the surface of cellulose. The chemical structure containing hydroxyl groups available for the modifications in order to improve surface interaction and enhance the barrier properties (Hubbe *et al.*, 2008; Rodionova *et al.*, 2010; Phanthong *et al.*, 2018). Methods of surface modification are divided into three main categories: polymer grafting, chemical methods and adsorption methods (Sharma *et al.*, 2019; Shen *et al.*, 2020).

Methods based on polymer grafting are distinguished generally in two techniques named “grafting-from” and “grafting-to”. In the approach of “grafting-from”, the surface of cellulose is linked to a reactive group considered as an initiator for generating polymerization starting from a monomer, while in the technique “grafting-to”, a polymer chain that has already been functionalized with a reactive group at one end will attach to cellulose which is ready for the coupling. “Grafting-from” process, due to the different mechanisms, has a higher modification density than the “grafting-to” method (Hatton *et al.*, 2015; Chakrabarty and Teramoto, 2018). With polymer grafting methods, cellulose is linked to the polymer matrix by covalent bonds (Hatton *et al.*, 2015). However, these technologies have disadvantage in which they are processing with organic solvents and inert space which is difficult in industrial scale.

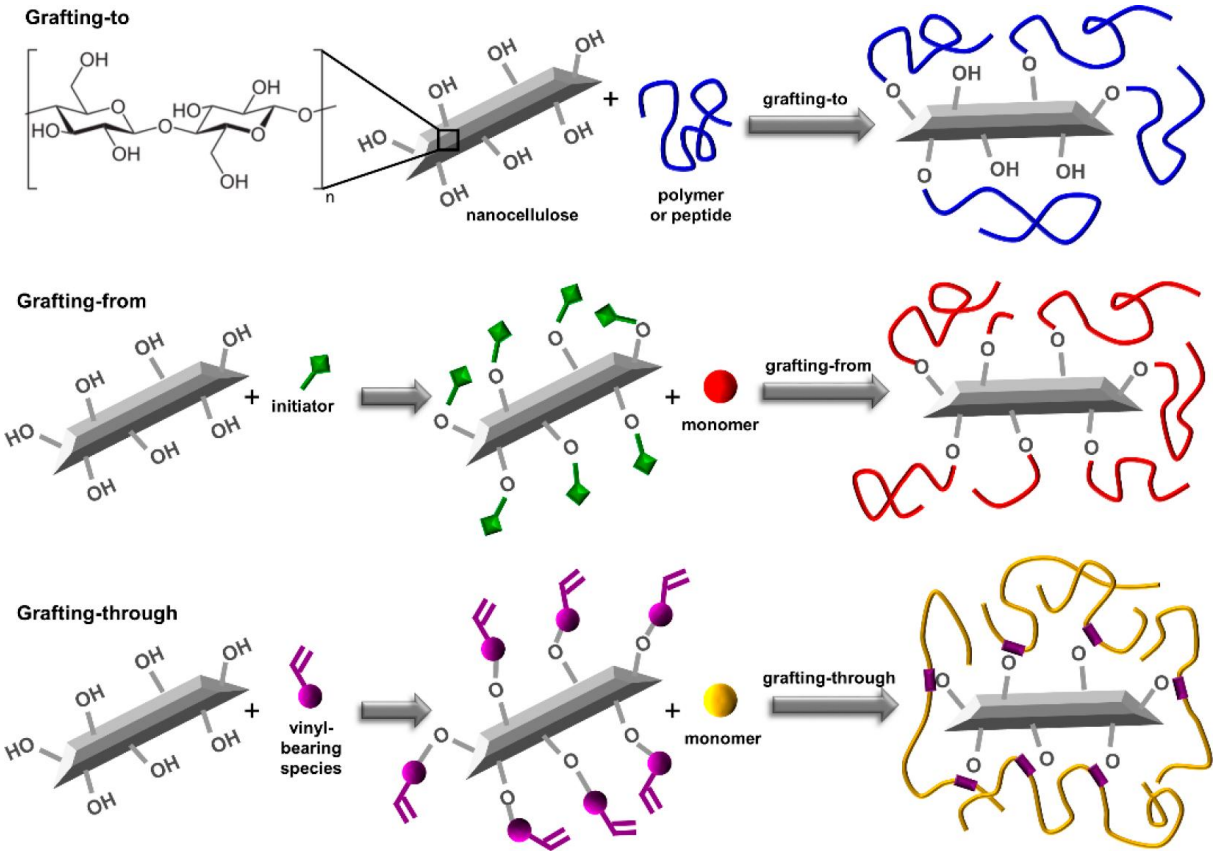

Figure 2.3.2.1 Polymer grafting methods (Thomas *et al.*, 2018).

Chemical modification is achieved by a direct interaction between cellulose filler and polymer without using any surfactants or coupling agents. The reactions, such as esterification, etherification, silylation, urethanization, amidation, are based on covalent or ionic bonds by interaction of hydroxyl groups on cellulose and compounds which have suitable reactive groups (Shen *et al.*, 2020; Sharma *et al.*, 2019; Thomas *et al.*, 2018).

In a larger production size in industry, physical adsorption is employed to adsorb polymer on cellulose surface. Polymeric materials used include uncharged polymers, which are called non-polyelectrolytes (non-PE) and polyelectrolytes (PE) that have charges on the polymer chain. Non-PEs are adsorbed on cellulose surface by Van der Waals and hydrogen bonds, while cationic PEs are found to be attached on cellulose by electrostatic interactions with negative charges on cellulose surface modified by carboxylation of hydroxyl groups (Hatton *et al.*, 2015).

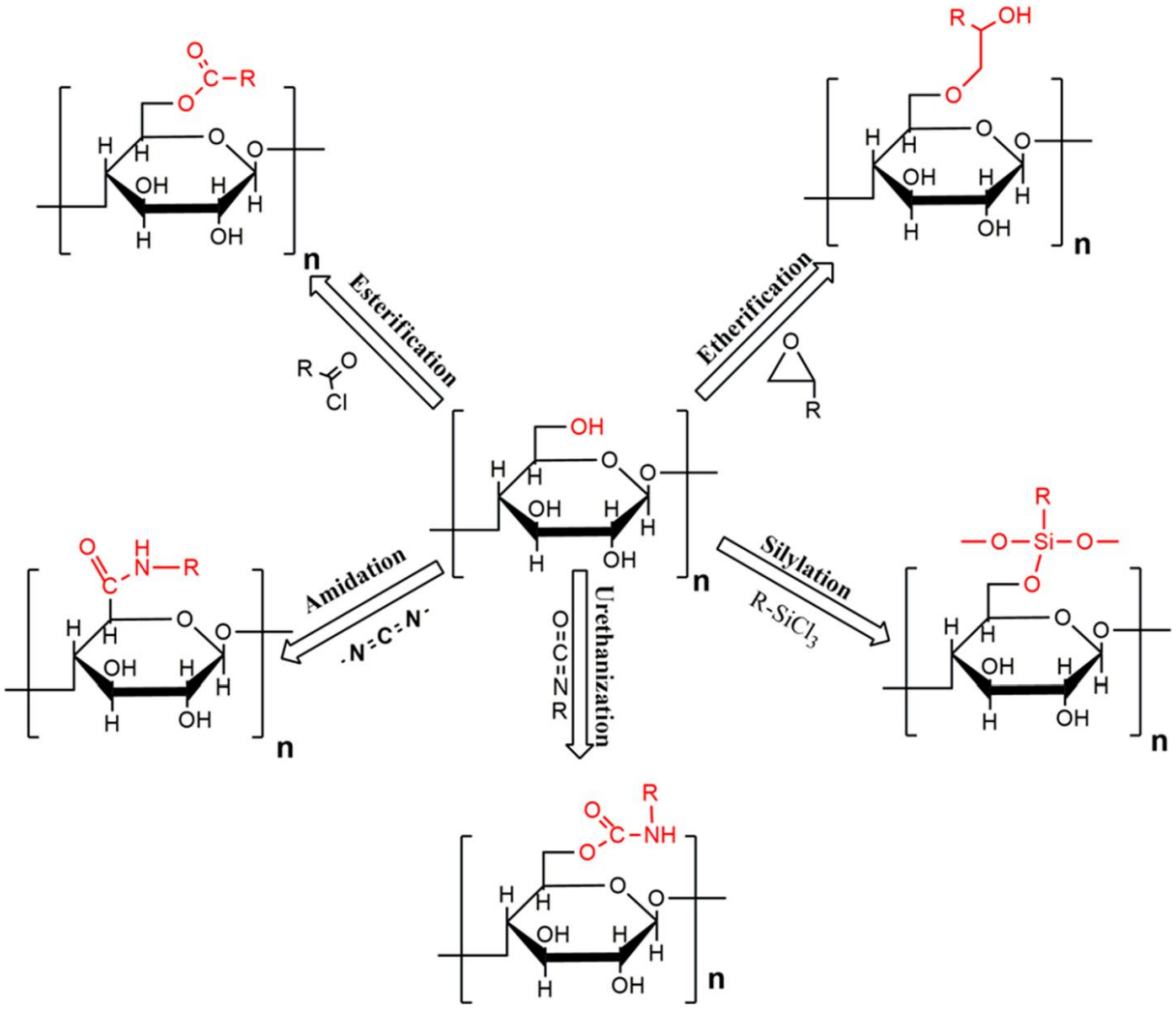

Figure 2.3.2.2 Surface modifications for creating hydrophobicity to nanocellulose surface (Thomas *et al.*, 2018).

3. Gas permeability in polymers and composites

3.1 Definitions

The global consumption of packaging is expected to reach $1.05 trillion in 2024, showing the importance of packaging in industry. The development and innovation in processing methods for packaging materials are thus required, which would greatly affect the quality, taste, longevity and marketability for the products during harvest, transportation and storage (Smithers, 2019). Packaging materials provide barrier properties, heat resistance, mechanical strength for the preservation of goods, but also result in the concerns of packaging disposal and the subsequent environmental impact. The conventional materials used for food packaging are from glass, metals. Metals and glass are very resistant to the permeability of oxygen and moisture but consume a lot of energy in the recycling process, incur high transportation costs and gradually accumulate in landfill as they are non-decomposable. Metal and glass cause damage to the environment and harm the atmosphere, animals, and marine life. To help environmental protection, industrial ecology and sustainability, bioplastics such as cellulose, polylactide, starch-based materials are developed and widely applied in packaging industry due to their biodegradability, renewability and biocompatibility (Wang *et al.*, 2017; Ferrer *et al.*, 2015).

Biodegradable polymers, which can be decomposed into CO_2, CH_4, H_2O and biomass through biocatalyst processes by microorganisms, can be conducted in decomposition processing to constitute compost. Unfortunately, they are brittle, thermally unstable, and have low melt strength and low resistance toward water vapor and oxygen permeation, which prevent widespread usage in packaging. On the other hand, nanocelluloses with nanoscale dimensions and high crystalline nature with hydrogen bonds allow the formation of very strong molecular networks, making them very sturdy and preventing molecules from passing through. The addition of nanocellulose into biopolymers both improves the mechanical properties such as tensile strength (around 104–154 MPa) and Young's modulus (15.7–17.5 GPa) and enhances the barrier properties for materials, which are vital for packaging applications (Peelman *et al.*, 2013; Wang *et al.*, 2017).

One of the most important characteristics of packaging materials is the prevention of contact between product and the environment, e.g. transmission of oxygen and moisture. This characteristic is referred as chemical protection, minimizing the changes in chemical composition of the product during storage time (Marsh and Bugusu, 2007). Oxygen molecule has diameter of $2.98*10^{-8}$ cm; therefore, materials' structure with larger pore size would allow oxygen to easily pass through and have high oxygen permeability.

The permeation of a gas phase includes three basic phenomena: the diffusion of the gas phase through a material, the absorption and desorption. The permeant is firstly dissolved into the upstream surface of the material, then passes through the film or membrane to reach the downstream side by a diffusion process from high to low concentration regions, then exits and evaporates again. The mechanism above is described mainly by solubility and diffusion. The gas permeability through material; therefore, is expressed by:

$$P = D \times S$$

Where:

- P is the permeability.

- D is the diffusion coefficient.
- S is the solubility coefficient.

Then applying Henry's law of solubility and Fick's first law of diffusion:

$$J = \frac{q}{A \times t} = -D \times \frac{\partial c}{\partial x}$$

$$\Delta p = \frac{\Delta c}{S}$$

where:

- J is the diffusion flux
- Δc is the concentration difference between two sides of film or membrane.
- x is the direction of mass transport
- q is the amount of gas phase passing through material.
- l is the thickness of film or membrane of material.
- A is the cross-section area.
- t is the observed time.
- Δp is the pressure difference between two sides of film or membrane.

We have:

$$P = D \times S = \frac{ql}{A \times t \times \Delta p}$$

The permeability is usually measured by three parameters: permeance, transmission rate and permeability. Transmission rate is the amount of permeant passing through a material per unit of surface area and unit of time under the equilibrium conditions applied. The amount is usually given in volume units for oxygen and in weight units for water vapour. Permeance is the transmission rate divided by the partial pressure difference of the permeant between the two sides of the film. Finally, the permeability is calculated by the permeance multiplied by the thickness of the material that the permeant is passing through.

Table 3.1.1 Barrier properties, equations and unit

Barrier property	Equation	Unit
Oxygen Transmission Rate (OTR)	$OTR = \frac{\text{Volume passed through}}{\text{area} \times \text{time}}$	$cm^3/m^2.day$
Oxygen Permeance	$\text{Permeance} = \frac{OTR}{\text{oxygen partial pressure difference}}$	$cm^3/m^2.day.atm$
Oxygen Permeability (OP)	$OP = \frac{OTR \times \text{thickness}}{\text{oxygen partial pressure difference}}$	$cm^3.\mu m/m^2.day.atm$
Water vapor Transmission Rate (WVTR)	$WVTR = \frac{\text{Weight passed through}}{\text{area} \times \text{time}}$	$g/m^2.day$
Water vapor Permeance	$\text{Permeance} = \frac{WVTR}{\text{saturated pressure} \times \Delta\%RH}$	$g/m^2.day.kPa$
Water vapor Permeability (WVP)	$WVP = \frac{WVTR \times \text{thickness}}{\text{saturated pressure} \times \Delta\%RH}$	$g.\mu m/m^2.day.kPa$

Barrier properties depend not only on the material but also on the surrounding atmosphere, and particularly on temperature, pressure and relative humidity. Besides, the transmission rate and the permeance also vary with thickness of the material and the partial pressure of the permeant between two sides of the interface. When the conditions of the test and the thickness of the material are given, the transmission rate, the permeance and the permeability can be converted into one another. The permeability is often expressed in the unit of ($cm^3.\mu m/m^2.day.atm$) for oxygen and ($g.\mu m/m^2.day.kPa$) for moisture in literature. By these units, the thicknesses of films are necessarily given.

There are different methods to measure the transmission of oxygen gas and moisture. The methods reported in this research focus on just the measurement of oxygen gas transmission including ASTM D3985, ASTM F1927, ASTM F1307, ASTM F3136, and ASTM F2622. Depending on each method, different conditions and equipments would be applied, leading to different results. ASTM D3985 and ASTM F1927 are the most frequently used methods (Wang *et al.*, 2017).

Both methods of ASTM D3985 and ASTM F1927 use plastics in the form of film or sheeting as specimen. The film specimen is mounted as a sealed semi-barrier between two chambers at atmospheric pressure. One chamber is purged by nitrogen stream and the other contains oxygen. Nitrogen carrier gas contains mixture of nitrogen and hydrogen in dry condition where hydrogen occupies 0.5 – 3 % volume fraction. Oxygen test gas contains oxygen with at least 99.5 % concentration. After the sample has equilibrated in a given temperature and humidity condition, oxygen is switched into the test-gas side. ASTM D3985 is tested in dry condition at 23 ^oC while ASTM F1927 is usable with any controlled temperature and a broad range of humidity level from 0 – 90 %RH. The measurement occurs in 30 – 60 min for thin films or several hours or days for thicker and more complex specimen to reach the steady state of gas transmission. Oxygen is permeated through specimen, passes nitrogen chamber and being transported to coulometric detector, producing an electric current which has

magnitude proportional to the amount of detected oxygen per unit of time. The detector provides a linear output which followes Faraday's law, produces four electrons for each molecule of passing oxygen into it. With an efficiency of 95 – 98% ASTM D3985 and ASTM F1927 are considered to be reference methods for measuring the oxygen transmission rate (ASTM D3985, 2017; ASTM F1927, 2020). The oxygen transmission rate is determined by the following equation:

$$OTR = \frac{(E_e - E_0) \times Q}{A \times R_L}$$

Where:

- E_0 is the observed steady state voltage at zero-level before oxygen passing through.
- E_e is the observed steady state voltage after oxygen passing through.
- A is the area if the specimen.
- R_L is the value of load resistance in which passes the current from the coulometric device.
- Q is the calibration constant for calculating OTR.

Similar to ASTM D3985, test method ASTM F1307 uses an analogous arrangement of equipments. The method is applied for the oxygen transmission rate measurement of packages such as bottles, cups or pouches. The package is mounted on a test fixture where inside of the package is purged by nitrogen stream and the outside is exposed to oxygen. The package is tested at either ambient room air of 20.8% oxygen or at 100% oxygen concentration, with oxygen pressure controlled at atmospheric pressure. Temperature and relative humidity are also controlled (ASTM F1307, 2020).

ASTM F3136 method is applied for plastic films, sheeting and laminates as well. The tested film is mounted between two chambers; the sensing well containing oxygen sensor is purged by pure nitrogen stream. The opposite chamber which is driving well is exposed to air or pure oxygen. Instead of using coulometric detector, ASTM F3136 utilizes a method called dynamic accumulation for determining oxygen transmission rate. This method measures the oxygen concentration periodically and accumulates the recorded data by using an oxygen sensor incorporates with a fluorophore which fluoresces responding to wavelength of light and being quenched in the presence of oxygen. The fluorescent signal extinction depends on the oxygen partial pressure. The permeation of oxygen is calculated by:

$$\ln\left(\frac{\Delta p_{O_2}^{initial}}{\Delta p_{O_2}^{time=t}}\right) = \frac{OTR \times Area}{Volume} \times time$$

where:

- $\Delta p_{O_2}^{initial}$ is the partial pressure difference of oxygen passes through the film at time 0.
- $\Delta p_{O_2}^{time=t}$ is the partial pressure difference of oxygen passes through the film at any time t.

- OTR is oxygen transmission rate.
- Area is the film area.
- Volume of sensing well.
- Time is in unit time.

After periodically recording the data corresponding at each time t, oxygen transmission rate is determined by:

$$\mathrm{OTR} = \frac{|\mathrm{Slope}| \times \mathrm{Volume}}{\mathrm{Area}}$$

The slope is obtained from the graph of calculated variables versus time. The unit of OTR is obtained in ($cm^3/(m^2.day)$). However, in the end, this test method is not guaranteed since the tested materials are limited and the expected accuracy of 95% can be decreased (ASTM F3136, 2015).

A more general method to determine oxygen transmission applied for processes with varying devices, instruments and procedures is ASTM F2622. This test method uses specimen of a plastics film, sheeting, laminate or plastic-coated paper. Similar to other methods, the specimen is mounted as a sealed semi-barrier between two chambers; one chamber is purged by nitrogen stream and the other contains oxygen. Oxygen passes the film, moves into the purged chamber and being transported to the detector where it produces signal representing transmission rate. The surrounding environmental conditions including temperature, humidity level and oxygen concentration in both chambers must be controlled since their fluctuations can affect the measurement significantly (ASTM F2622, 2020).

Table 3.1.2 Summary of ASTM standards

Test method	Material	Temperature	Relative humidity	Device
ASTM D3985	Plastic films	23°C	< 1 %	Coulometric detector
ASTM F1927	Plastic films	Any controlled temperature	0 – 90 %	Coulometric detector
ASTM F1307	Packages	Ambient	-	Coulometric detector
ASTM F3136	Plastic films	Controlled	-	Oxygen sensor + fluorophore
ASTM F2622	Plastic films	Controlled	Controlled	Various detectors

Even though the evaluation and classification for barrier properties of materials have not been implemented sufficiently yet due to the dependence on film thickness and different methods, According to ASTM D3985 (2017), ASTM F1927 (2020), ASTM F1307 (2020), ASTM F2622 (2020), materials which have transmission rate over 200 $cm^3/(m^2.day)$ with partial pressure difference of one atmosphere are considered to be poor barrier. ASTM F3136 (2015)

reports that materials with transmission rate higher than 100 $cm^3/(m^2.day)$ have poor barrier property and those with medium level range from 2 to 100 $cm^3/(m^2.day)$.

Table 3.1.3 Oxygen barrier property level in ASTM

Test method	Level	Value
ASTM D3985, F1927, F1307, F2622	Poor	Over 200 $cm^3/(m^2.day)$
ASTM F3136	Poor	Over 100 $cm^3/(m^2.day)$
	Medium	2 to 100 $cm^3/(m^2.day)$

Another test method used to measure the permeability of a general gas through plastic films or sheeting is ASTM D1434. The film is mounted as sealed semi-barrier between two chambers where the chamber containing the permeant has a specific high pressure and the other chamber which receives the permeanting gas has lower pressure. Two possible procedures could be utilized for the measurement: Manometric and Volumetric. In manometric procedure, the chamber with low pressure is firstly discharged and the increase of pressure expresses the transmission of gas through the film. In volumetric procedure, the transmission of gas is expressed by the changing of volume when the low-pressure chamber is adjusted to near atmospheric pressure. The process occurs in condition of 23 ± 2^0C and the humidity of the test gas does not change (ASTM D1434, 2015).

3.2 Collection of permeability data for polymers

Oxygen barrier packaging is one of the mandatory requirements for packaging industry of goods such as food, beverages and pharmaceuticals, in order to protect the product, avoid reaction of oxidation and aerobic microbiological growth. Since the introduction of plastics in packaging, polymer chemistry and technology have been developed for oxygen barrier properties including changing formulation and adding compatible chemicals. In fact, some polymers which are used for oxygen barrier packaging have already been in commercial use since 1978. For example: Polyvinyl alcohol (PVOH), ethylene vinyl alcohol (EVOH), polyvinylidene chloride (PVDC), Nylons, Acrylonitrile (PAN), polyethylene terephthalate (PET), polyethylene naphthalate (PEN), Polytrimethyl Terephthalate (PTT) and liquid crystal polymers (LCPs) (Strupinsky and Brody, 1998).

The main factor in deciding barrier properties of polymers is chemistry, which means by changing the structure and chemical position the barrier properties can increase or decrease by more than five orders of magnitude. The properties of polymers are determined by the functional group on the chain. Therefore, by adjusting pendant groups, which affect the affinity between permeant and polymer matrix, significant variations of barrier properties of polymers are obtained.

Diffusion is the main mechanism with which the gas phase passes through a film material; therefore, polymers have high barrier properties when they have a low diffusion coefficient, which is influenced by both static and dynamic effects. Static effects consist of molecular packing, which controls the free volume, morphologies and molecular architecture. Free volume is the empty space between the polymer chains which allow permeant to diffuse in. The larger the free volume, the more easily permeant can enter. Morphologies of polymers are of two types: crystalline and amorphous. While crystallinity makes the diffusion difficult,

polymers do not exist fully in crystalline form; instead, some polymers exist in amorphous form. Molecular architecture of polymers including branches and molecular weight controls the diffusion of gas phase, which affects their barrier properties (Lagaron *et al.*, 2004; DeLassus, 2002).

Dynamic effects are the result of polymer chain mobility. This is the movement of free volume inside polymers. The chains move with thermal motion facilitating the diffusion. This effect is related to the glass transition temperature Tg of a polymer. Below Tg, thermal motion is limited, free volume between polymer molecules are small, preventing permeant from passing through. When temperature increases and surpasses Tg, thermal motion increases and free volume between polymer molecules enlarges, reducing the impermeability of polymers (DeLassus, 2002).

A collection of oxygen permeability data of polymers are reported in the Table.

Table 3.2.1 Oxygen permeability data of thermoplastic and thermosetting polymers

Reference	Name	Type	Permeability (cc $\mu m\ m^{-2}\ day^{-1} kPa^{-1}$)	Method	Instrument	Temperature (^0C)	RH (%)
Maes *et al.*, 2019	Poly(Vinyl Alcohol) (PVOH)	Thermoplastic	0.0148	-	-	23	0
Maes *et al.*, 2020	Polyvinylidene chloride (PVDC)	Thermoplastic	0.1-2.96	-	-	23	50
Chaos *et al.*, 2019	Polyhydroxybutyrate (PHB)	Thermoplastic	6.496	ASTM D3985	MOCON OX-TRAN 2/21 MH	23	0
Huang *et al.*, 2004	Polyamide 6 (PA-6)	Thermoplastic	17.0738	ASTM D1436	Lyssy L-100-5002	23	0
Maxwell and Roberts, 2009	Polyester cross-linked	Thermoset	17.5398	-	-	25	-
Djordjevic *et al.*, 2016	Polyethylene (PE) + Polycaprolactone (PCL) as binder	Thermoplastic	21.198	DIN 53380	Lyssy GPM-200	23	-
Keller and Kouzes, 2017	Polyamide 66 (PA-66)	Thermoplastic	22.0084	-	-	-	-

Table 3.2.1 (Cont.) Oxygen permeability data of thermoplastic and thermosetting polymers

Reference	Name	Type	Permeability (cc μm m^{-2} day^{-1} kPa^{-1})	Method	Instrument	Temperature (^{0}C)	RH (%)
Keller and Kouzes, 2018	Polyvinyl chloride (PVC)	Thermoplastic	32.371-3888.478	-	-	-	-
Sekelik *et al.*, 1999	Polyethylene terephthalate (PET)	Thermoplastic	38.49	ASTM D3985	MOCON OX-TRAN 2/20	25	0
Maxwell and Roberts, 2008	Epoxy-amine	Thermoset	83.1519	-	-	30	-
Chaos *et al.*, 2018	Poly (l-lactic acid) (PLLA)	Thermoplastic	90.9474	ASTM D3985	MOCON OX-TRAN 2/21 MH	23	0
Huang *et al.*, 2004	High-density polyethylene (HDPE)	Thermoplastic	91.5865	ASTM D1435	Lyssy L-100-5001	23	0
Keller and Kouzes, 2017	Polystyrene (PS)	Thermoplastic	972.119-1687.639	-	-	-	-
Zhang *et al.*, 1993	Polylactic acid (PLA)	Thermoplastic	318.3814458 ± 12.23784851	ASTM D3985	MOCON Model 702	23	0
Jung *et al.*, 2020	Aromatic Polyester	Thermoset	1039.4	-	K-315-N	30	-

The permeability of polymers are obtained in different units. For example: In SI unit, the permeability is measured in (amol.m^{-1}.s.Pa), or in Barrer, which is (cc.cm.cm^{-2}.s.(cmHg)).10^{-10} or in metric unit of (ml.mil.m^{-2}.d.atm). However, in this thesis, all the oxygen permeability

values of all the materials are converted into unit of ($cc.\mu m.m^{-2}.day^{-1}.kPa^{-1}$) by multiplying and dividing each conversion factor in order to reach the amount of volume of a permeant; in this case it is Oxygen in cubic centimeters, that passes through a film with a specific thickness of micrometers made in thermoplastic or thermosetting type of polymer that is normalized in a unit of film surface, pressure difference measured in kilopascals in one day. Each case is measured with different methods, different instruments and different environmental conditions.

Among the polymers reported, poly (Vinyl Alcohol) (PVOH) has the lowest oxygen permeability, i.e. 0.0148 ($cc.\mu m.m^{-2}.day^{-1}.kPa^{-1}$) at 23^0C and 0% RH. However, due to its low degradation temperature of 150 °C and high solubility in water, PVOH is not widely applied in packaging. Instead, PVOH can be used as coating material on other polymers to improve their barrier properties (Maes *et al.*, 2019). Polyvinylidene chloride (PVDC) has been considered a good barrier, and is used in fresh meat packaging based on its low oxygen permeability of 0.1-2.96 ($cc.\mu m.m^{-2}.day^{-1}.kPa^{-1}$) at room temperature and high relative humidity, i.e. 50% RH. Vinylidene chloride, which has the structure of symmetric 1,1 dichloroethene making adjacent molecular chains pack tightly together, preventing oxygen from passing through. Unfortunately, vinylidene chloride is not currently recyclable and its treatment damages the environment through releasing harmful substances like dioxins and hydrogen chloride (Krehalon, 2020). The non-polar polymers, for example, high-density polyethylene (HDPE), low-density polyethylene (LDPE) or polystyrene (PS), have oxygen permeability about three to four orders of magnitude higher than PVOH. The barrier properties of HDPE are improved by coupling it with polyamide 6 (Nylon 6) to create a three-layer film with various thickness fraction of Nylon 6. The oxygen permeability decreases with the increasing thickness fraction, with pure Nylon 6 at the lowest permeability: 91.6 ($cc.\mu m.m^{-2}.day^{-1}.kPa^{-1}$) for pure HDPE and 17.1 ($cc.\mu m.m^{-2}.day^{-1}.kPa^{-1}$) for pure Nylon 6 (Huang *et al.*, 2004). Polyethylene terephthalate (PET) has oxygen permeability of 38.49 ($cc.\mu m.m^{-2}.day^{-1}.kPa^{-1}$), and thus considered to be a good barrier. PET is one of the most employed materials in packaging such as beer, fruit juices, soft drinks, frozen products. In order to enhance the barrier properties, it is coated with Polyphenols and Gelatin mixture to form a multilayer structure (Ishtiaque *et al.*, 2018).

Compared to synthetic plastics, natural polymers with biodegradable properties attract more development regarding sustainable technologies due to their environmental safety. Natural polymers decrease the dependence on fossil fuel as carbon source and reduce the significant amount of hazardous wastes caused by non-biodegradable plastics. Polyhydroxybutyrate (PHB) is a biodegradable polymer, which is known as the first identified type in polyhydroxyalkanoates (PHAs) family (Gangurde and Sayyed, 2012). PHB has excellent barrier properties with oxygen permeability of 6.496 ($cc.\mu m.m^{-2}.day^{-1}.kPa^{-1}$). Unfortunately, PHB has a high degree of crystallinity, which makes them very stiff and brittle. It was then found that by adding plasticizers such as tributyl citrate (TbC), PHB can become more ductile and easier to be processed (Chaos *et al.*, 2018).

Another polymer that has been studied extensively among biodegradable polymers is Polylactic acid (PLA). PLA is thermoplastic polyester which has many advantages: it is compostable, has high strength and stiffness and good biocompatibility with fresh products. Depending on measuring conditions, PLA's oxygen permeability values vary in a broad range from 90.9474 ($cc.\mu m.m^{-2}.day^{-1}.kPa^{-1}$) at 23 ^{0}C and 0 %RH to 1183.7 ($cc.\mu m.m^{-2}.day^{-1}.kPa^{-1}$) at 24 ^{0}C and 80 %RH (Chaos *et al.*, 2018; Sanchez-Garcia and Lagaron, 2010). Furthermore, in similar measuring conditions of 23 ^{0}C and 0 %RH, there are disparities in the results: 90.9474 ($cc.\mu m.m^{-2}.day^{-1}.kPa^{-1}$) (Chaos *et al.*, 2018) and 318.38 ($cc.\mu m.m^{-2}.day^{-1}.kPa^{-1}$)

(Jung *et al.*, 2020). The main drawback of PLA is its brittleness, low thermal resistance and low impermeability, which in turn limit its applications in packaging.

The barrier properties of polymers, however, are limited compared to materials used in food packaging like glass and tinplate, since they allow compounds with low molecular weight such as gases and vapor to pass through. Therefore, polymers are not utilized in applications requiring high degree of impermeability. However, due to their adaptability with various properties, low price and flexibility of shapes and size, polymers garner great interest from researchers to further develop and overcome their limitations in impermeability properties.

3.3 Collection of permeability data in composites with cellulosic fillers

Polymers incorporating nanocellulose are found to be advantageous in improving the permeability compared with polymers themselves. Nanocelluloses are particularly used in combination with biobased polymers as both the filler and the matrix are environmentally friendly. Poly lactic acid (PLA) is observed to be an attractive polymer when it is used as the reinforced matrix for nanocellulose filler.

Jung *et al.* (2020) used melt mixing method to incorporate PLA with freeze dried cellulose nanofibers (CNFs). PLA is preliminarily dried in a vacuum oven for 12 hours at 80 ^{0}C; afterwards it was melted at 180 ^{0}C for one minute. Freeze-dried CNFs were then added and mixed at 50 rpm rotation speed to produce freeze-dried CNF/PLA nanocomposites. CNFs find difficulty in being well dispersed in polymers, especially in non-polar polymers like PLA, they tend to agglomerate creating a non uniform material. Another method is by adding eco-friendly plasticizers such as triethyl citrate (TEC), CNFs can be uniformly immersed in the matrix, enhancing tensile strength and flexibility of the composite. By mixing PLA with freeze-dried CNFs of 20-60nm in width and several micrometers in length, the oxygen barrier properties increased with the permeability value of 318.38, 311.37, 222.26 (cc.µm.m^{-2}.day^{-1} .kPa^{-1}) when the volume fraction of CNFs increased from 0 vol%, 0.21 vol%, 0.41 vol%, respectively . The measurement of oxygen transmission rate is applied by method ASTM D3985. Notably, when volume fraction of CNFs increases to 0.83vol%, permeability value increases to 284.7 (cc.µm.m^{-2}.day^{-1} .kPa^{-1}). This result is believed to be caused by the agglomeration of CNFs when the amount of CNFs increases (Jung *et al.*, 2020).

Sanchez-Garcia and Lagaron (2010) similarly used PLA as Jung *et al.* (2020) to produce nanocomposites with cellulose nanowhiskers (CNWs) by casting from chloroform solution. CNWs are prepared by acid hydrolysis from highly purified alpha microcrystalline cellulose (MCC) having thickness of 10 – 20 nm and length of 60 – 160 nm. MCC of 10 g/100 mL was hydrolyzed in 9.1 mol/L sulphuric acid at 44 ^{0}C for 130 minutes. After that, the excess of sulphuric acid was removed by centrifugation and the supernatant was replaced by deionized water. The CNW suspension by now has pH of 3.5, and gradually being neutralized by slowly adding sodium hydroxide until obtaining pH of 7. The suspension was then freeze-dried, chloroform was directly added and mixed in a homogenizer. Chloroform CNW suspension was stirred with PLA for 30 minutes at 40 ^{0}C, producing nanocomposite of 100µm thickness. The oxygen permeability is measured in conditions of 24 ^{0}C and 80 %RH obtained decreasing values with increasing volume fraction of CNWs. The permeability values for 0 vol%, 0.83 vol%, 1.67 vol%, 2.5 vol% are 1183.7, 198.7, 121, 129.6 (cc.µm.m^{-2}.day^{-1} .kPa^{-1}) respectively. When the volume fraction of CNW increases to 4.17 vol%, the permeability value increases to 138.24 (cc.µm.m^{-2}.day^{-1} .kPa^{-1}) due to the agglomeration of CNW in the matrix (Sanchez-Garcia and Lagaron, 2010).

Martínez-Sanz *et al.* (2013) prepared nanocomposites composed of bacterial cellulose nanowhiskers (BCNW) films coated with PLA. Bacterial cellulose mats were firstly obtained by incubating Gluconacetobacter xylinus 7351 in Hestrin-Shramm medium at 30 ^{0}C. The bacterial cellulose pellicles were sterilized in boiling water, cleaned in a 10 vol% of sodium hydroxide aqueous solution and then blended as gel-like material. Afterwards the suspension was compressed to remove absorbed water. Bacterial cellulose nanowhiskers (BCNW) were obtained by mixing dried bacterial cellulose with 301 mL sulphuric acid/L water, in a amount of 7 g cellulose/L acid for three days at 50 ^{0}C. The homogeneous solution was then precipitated under process of centrifugation for 20 minutes at 15 ^{0}C and 12,500 rpm. The white precipitate was subsequently re-suspended and neutralized in deionized water and sodium hydroxide until reaching neutral pH, followed by centrifugation to acquire partially hydrated precipitate.

The composite was obtained by electrospinning BCNW films coated with PLA mats. A solution of PLA and 1,1,1,3,3,3-hexafluoro-2-propanol (HFP) were transported to plastic syringe of 5 mL connected by stainless steel needle of 0.9 mm in diameter. An electrode connected to a high voltage power supply of 10 – 12 kV was clamped to the needle tip where polymer solution was fed at 0.66 mL/h. BCNW film was placed on a circular plate connected to the counter electrode, with 6 cm far from the needle. The electrospinning occurs at ambient temperature. The composite product of bacterial cellulose nanowhisker (BCNW) films coated with PLA was found to have oxygen permeability decreases 97% compared to the BCNW film itself in the humidity condition of 80 %RH and 24 ^{0}C. Additional specimen was prepared by adding 20 wt% polyethylene glycol (PEG) to BCNW. The film was tested at 24 ^{0}C in humidity conditions of 0 %RH and 80 %RH. The measured permeability increases enormously in the condition of 0 %RH; however, at 80 %RH it increases significantly (from 0.035 to 619 ($cc.\mu m.m^{-2}.day^{-1}.kPa^{-1}$)) (Martínez-Sanz *et al.*, 2013).

Djordjevic *et al.* (2016) prepared polyethylene (PE) coated with dispersion of cellulose nanocrystals (CNCs) and polycaprolactone (PCL) as binder. Cellulose nanocrystals (CNCs) were prepared by mixing 20 g of cotton with 200 mL of sulphuric acid (64 wt %); the solution was hydrolyzed under continuous stirring for 60 min at 40 °C. Afterwards, it was centrifuged at 5000 rpm for 20 minutes by adding 1000 mL of water. The supernatant was removed, followed by sonification and centrifugation processes with deionized water in order to obtain pH value of 4 of the supernatant. Dialysis was then conducted to acquire water at pH of 5. The composite dispersions were prepared by mixing polycaprolactone (PCL) with CNC at 800 rpm for 30 minutes, followed by ultrasound treatment at 30 – 35 ºC for 15 minutes and grinding at 12000 rpm for 5 minutes. The dispersions were then layered on the PE surface. Different thicknesses of the film with various CNCs content were prepared. The pure polymer has thickness of 60 µm. When the content of cellulose nanocrystals increases to 5 wt%, the film thickness is 12 µm. With 10 wt% of nanocellulose, the composite has thickness of 11 µm and with 15 wt% of nanocellulose, the thickness of the film is 14 µm. The oxygen barrier properties are enhanced when CNCs content increases (Djordjevic et al., 2016).

Galland *et al.* (2014) produced nanocomposites consist of cellulose nanofibers (NFCs) in photopolymerizable hyperbranched acrylate matrix (HBP). NCF was prepared in aqueous gel-like suspension using microfluidizer, subsequently diluted in deionized water with 0.2 wt % and stirred for 10 minutes. Afterwards, the suspension was degassed for 10 minutes in a vacuum chamber and subjected to vacuum filtration using membrane with pores of 0.65 µm to obtain wet NCF template. The template was then immersed in a solvent of ethanol and toluene with 95:5 wt % for one hour repeating three times with fresh solvent in order to guarantee complete solvent exchange. The template was immersed in a solvent of ethanol and toluene for 2 hours where HBP was dissolved, followed by the evaporation of solvent for 30

minutes at 60 ºC and for 2 hours at 120 ºC. Lastly, the nanocomposite film of 60 – 120 µm in thickness was polymerized for 3 minutes under UV radiation at an intensity of 50 mW/cm^2, using a 200 W mercury bulb UV lamp. Galland *et al.* (2014) demonstrated that the content of cellulose nanofibers (NFCs) in HBP matrix can change the permeability of oxygen at 23 °C and 0 %RH. The values decrease significantly with the increase of NFCs volume fraction.

Table 3.3.1 Oxygen permeability data of nanocomposites

	Nanocellulose	Polymer		Composite		Permeability			
Reference	Type of nanocellulose	Name	Type	Production method	Cellulose (vol%)	Permeability (cc mm m^{-2} day^{-1} kPa^{-1})	Instrument	Temperature (°C)	RH (%)
Galland *et al.*, 2014	Nanofibrillated cellulose (NFCs)	Hyperbranched polyester acrylate oligomer CN2302 (Sartomer)	Photocurable	-	0	37	oxygen permeation analyzer (Systech 8001)	23	0
				Solvent exchange+ UV curing	10	ca 20		23	0
					40	ca 10		23	0
					60	ca 9		23	0
				-	100	0.002		23	0
Martínez-Sanz *et al.*, 2013	Bacteria Cellulose nanocrystals (BCNWs)	The semicrystalline polylactide (PLA)	Thermoplastic	Electrospinning technique	41.7 - 50	17.28	Oxtran 100 equipment	24	80
								24	80
		polyethylene glycol 900 (PEG)			66.7	0.035		24	0
						619		24	80
Jung *et al.*, 2020	Cellulose nanofibers (CNFs)	Poly lactic acid (PLA)	Thermoplastic	-	0	318.38 ± 12.24	oxygen transmission rate analyzer (Model: 702, MOCON)	23	0
				Melt mixing	0.21	311.37		23	0
					0.41	222.26		23	0
					0.83	294.7		23	0

Table 3.3.1 (Cont.) Oxygen permeability data of nanocomposites

	Nanocellulose	Polymer		Composite		Permeability			
Reference	Type of nanocellulose	Name	Type	Production method	Cellulose (vol %)	Permeability (cc mm m^{-2} day^{-1} kPa^{-1})	Instrument	Temperature (°C)	RH (%)
Djordjevic *et al.*, 2016	Nanocellulose nanocrystals (CNCs)	Polyethylene (PE) + Polycaprolactone (PCL) as binder	Thermo plastic	-	0	21.2	Lyssy GPM-200, Gasukuro Kogyo GC-320, HP 3396 integrator.	23	-
				Mixing and layering	3.82	3.8		23	-
					7.63	3.2		23	-
					11.45	3.81		23	-
Sanchez-Garcia and Lagaron, 2010	Cellulose nanowhiskers (CNWs)	Poly(lactic acid) (PLA)	Thermo plastic	-	0	1183.7	Oxtran 100 equipment	24	80
				Chloroform casting	0.83	198.7		24	80
					1.67	121		24	80
					2.5	129.6		24	80
					4.17	138.24		24	80

4. Modeling gas permeability

4.1 Models presented in literature

Even though no model has been specifically developed for estimating the oxygen permeability of nanocellulose composites yet, several empirical and semi-empirical models were presented for predicting permeation properties of polymer-based composites (Prasad *et al.*, 2021). Empirical models are based on the fitting of experimental data with e.g. polynomial equations, without considering the physical processes involved, thus can only be applied when the same conditions are respected. Instead, semi-empirical models are based on the combination of empirical parameters from fitting of experimental data and simplified mathematical expressions of physical principles. They can be applied in a larger set of conditions.

The most common empirical models used for predicting permeability for polymer blends and polymeric composites include the additive model, the ideal laminate model and the logarithmic model (Prasad *et al.*, 2021). The additive model, which is also called rule of mixtures, is the most basic and ideal model; it describes the permeation of composites in which the constituents do not interact with each other and the distances between particles are very large. This method is applicable for every system where the permeabilities of both the continuous (P_C) and the dispersed phase (P_D) are known (Prasad *et al.*, 2021), and the permeability P of the composite is calculated as:

$$P = (1 - \Phi_D)P_C + \Phi_D P_D \qquad \text{(Eq. 4.1.1)}$$

where Φ_D is volume fraction of the dispersed phase.

The ideal laminate model estimates the permeation through multi-layer films or laminates which are assumed homogeneous and defect-free. In this model the permeation of a gas through a multi-layer system is considered similar to the passage of electric current through resistors in series. The permeability is calculated from:

$$\frac{1}{P} = \frac{(1 - \Phi_D)}{P_C} + \frac{\Phi_D}{P_D} \qquad \text{(Eq. 4.1.2)}$$

or, in a more general way:

$$\frac{1}{P} = \sum_{i=1}^{i=n} \frac{\Phi_i}{P_i} \qquad \text{(Eq. 4.1.3)}$$

where Φ_i and P_i are the volume fraction and permeability of each layer and Φ_i/P_i is the resistance of the layer. Φ_i can be expressed as the ratio of thickness of each layer (h_i) over the total thickness (h):

$$\Phi_i = \frac{h_i}{h} \qquad \text{(Eq. 4.1.4)}$$

The last empirical model described here is the logarithmic model which may be applied for copolymers and filled polymers and is expressed as:

$$\log P = \Phi_C \log P_C + \Phi_D \log P_D \qquad \text{(Eq. 4.1.5)}$$

However, the empirical methods are found to be not accurate for the real systems (Mannan *et al.*, 2017), since they assume idealized materials in which the constituents do not interact with each other, which is not true for the majority of real systems. Therefore, it is necessary to implement semi-empirical models. These may be developed modifying the empirical ones introducing parameters that take into account the non-ideality of real systems, or they can be derived from models developed for other phenomena that are analogous to mass transfer.

Semi-empirical models based on the correlation of electric and thermal conductivity with mass transport have been proposed to predict the permeation properties of polymer composites (Prasad *et al.*, 2021). These models assume that the mass transport is controlled by diffusivity. One of the most widely used is the model from Maxwell (1873) (Gonzo *et al.*, 2005; Hashemifard *et al.*, 2009; Sanaeepur *et al.*, 2017; Rybak *et al.*, 2018; Shimekit *et al.*, 2010). The model initially developed by Maxwell for the dielectric properties of polymeric composites was extended to estimation of permeability:

$$P = P_C \frac{P_D + 2P_C - 2\Phi_D(P_C - P_D)}{P_D + 2P_C + \Phi_D(P_C - P_D)} \qquad \text{(Eq. 4.1.6)}$$

The model is used for ideal membranes which have no defects and are not affected by the interactions between near-by particles, thus is suitable for diluted suspensions of spherical particles with low volume fractions ($0 < \Phi_D < 0.2$) (Rybak *et al.*, 2018). It was e.g. applied for predicting the permeability of mixed matrix membranes (MMMs), i.e. separation membranes composed of two phases, in which inorganic particles, usually microporous or acting as molecular sieves, are immersed in a polymer matrix (Chung *et al.*, 2007).

A modification of the Maxwell model was proposed by Chiew and Glandt considering the effects of the interaction between the dispersed phase, represented by spherical particles, and the matrix, as well as the interaction between the particles themselves: the permeability was expressed as:

$$P = P_C \frac{1 + 2\beta\Phi + (K - 3\beta^2)\Phi^2}{1 - \beta\Phi} \qquad \text{(Eq. 4.1.7)}$$

where:

$$\beta = \frac{P_D - P_C}{P_D + 2P_C} \qquad \text{(Eq. 4.1.8)}$$

β describes the permeability difference between continuous and dispersed phase, which lies in the range $-0.5 \leq \beta \leq 1$. The lower bound defines perfectly non permeable particles and the upper bound corresponds to infinitely permeable particles (Chiew and Glandt, 1982; Gonzo *et al.*, 2005).

K is a correction factor depending on the shape and distribution of the particles, and is a function of both β and Φ. It is calculated by:

$$K = a + b\Phi^{3/2} \qquad \text{(Eq. 4.1.9)}$$

where a and b are functions of β:

$$a = -0.002254 - 0.123112\beta + 2.93656\beta^2 + 1.6904\beta^3 \qquad \text{(Eq. 4.1.10)}$$

$$b = 0.0039298 - 0.803494\beta - 2.16207\beta^2 + 6.48296\beta^3 + 5.27196\beta^4 \quad \text{(Eq. 4.1.11)}$$

Another set of models for thermal and electrical conductivity used to estimate the permeability of polymer composites include the ones from Bruggeman (1935), Bottcher (2010), and Pal (2008) (Prasad *et al.*, 2021; Gonzo *et al.*, 2005). Bruggeman model is particularly useful for composites which have nearly equal permeability values of dispersed and continuous phases, being treated as a uniform medium; therefore, ignores the effects of interaction between phases. Unlike Maxwell model, the Bruggeman one can be used for systems with high filler volume fraction using asymmetrical integration method from low filler volume fraction (Gonzo *et al.*, 2005):

$$(1 - \Phi_D) = \frac{P_D - P}{P_D - P_C}\left(\frac{P_C}{P}\right)^{1/d} \quad \text{(Eq. 4.1.12)}$$

The model is applicable for systems with random dispersed species where d indicates shape and size of particles. With spherical filler, d = 3. Bruggeman is an implicit model that needs to be solved numerically (Prasad *et al.*, 2021; Pal, 2007).

The Böttcher model (Böttcher, 2010) was modified to model permeability when the dispersed phase is composed by ellipsoidal particles:

$$\left(\frac{P_D}{P_C} + \frac{2P}{P_C}\right)\left(1 - \frac{P_C}{P}\right) = 3\Phi_D\left(\frac{P_C}{P} - 1\right) \quad \text{(Eq. 4.1.13)}$$

Pal model was originally developed for describing thermal conductivity of particulate composites, later it was adapted to predicting the permeability as:

$$P^{1/3} = \frac{\left(1 - \frac{\Phi_D}{\Phi_M}\right)^{-\Phi_M}}{\left(\frac{\frac{P_D}{P_C} - 1}{\frac{P_D}{P_C} - P}\right)} \quad \text{(Eq. 4.1.14)}$$

Φ_M is the maximum packing volume fraction of dispersed phase, which depends on shape, aspect ratio and orientation of particles (table 4.1.1). When $\Phi_M \rightarrow 1$, Pal model becomes Bruggeman model using spherical particles.

Table 4.1.1 Φ_M values for different dispersed phase (Nielsen, 1974).

Shape of dispersed phase	Configuration	Φ_M
Spheres	Hexagonal Close Packed	0.7405
Spheres	Face Centered Cube	0.7405
Spheres	Body Centered Cube	0.6
Spheres	Simple Cube	0.52
Spheres	Random Close	0.637
Spheres	Random Loose	0.601
Spheres	Uniaxial Hexagonal Close Packed	0.907
Rods/Fibres	Uniaxial Simple Cube	0.785
Rods/Fibres	Uniaxial Random	0.82
Rods/Fibres	3D Random	0.52

By taking into account the presence of an interfacial layer between dispersed phase and the continuous matrix, a modification of the original Pal model was obtained:

$$\left(\frac{P}{P_i}\right)^{1/3} = \frac{\left(1-\frac{\Phi_S}{\Phi_M}\right)^{-\Phi_M}}{\left(\frac{\frac{P_D}{P_i}-1}{\frac{P_D}{P_i}-\frac{P}{P_i}}\right)} \qquad \text{(Eq. 4.1.15)}$$

where:

$$\Phi_S = \frac{\Phi_D}{\Phi_D + \Phi_i} \qquad \text{(Eq. 4.1.16)}$$

in which Φ_i is the volume fraction of the interfacial polymer layer and P_i is the permeability of interfacial polymer region which becomes rigidified when in contact with filler surface (Pal, 2007).

Felske model is another approach based on thermal conductivity to predict the permeability of composites (Pal, 2007; Prasad *et al.*, 2021). It considers also the interaction between dispersed phase and continuous matrix. In particular, the permeability of interfacial shell P_I and radius of both outer interfacial shell and core are taken into account:

$$P = P_C\left[\frac{2(1-\Phi_D)+(1+2\Phi_D)\left(\frac{\beta}{\gamma}\right)}{(2+\Phi_D)+(1-\Phi_D)\left(\frac{\beta}{\gamma}\right)}\right] \qquad \text{(Eq. 4.1.17)}$$

$$\beta = \frac{(2+\delta^3)P_D-(1-\delta^3)P_I}{P_C} \qquad \text{(Eq. 4.1.18)}$$

$$\gamma = (1+2\delta^3)-(1-\delta^3)\frac{P_D}{P_I} \qquad \text{(Eq. 4.1.19)}$$

where δ is the ratio of interfacial shell outer radius to core radius. When $\delta \rightarrow 1$, Felske model approaches Maxwell model. It has the same limitation as Maxwell model regarding the volume fraction of the dispersed phase, so that for high volume fractions the results are

inaccurate (Prasad *et al.*, 2021). Therefore, a modification was proposed to prevent this disadvantage by considering the maximum packing fraction of the dispersed phase Φ_M (Pal, 2007).

$$P = P_C\left[\frac{1+2\left(\frac{\beta-\gamma}{\beta+2\gamma}\right)\Phi_D}{1-\left(\frac{\beta-\gamma}{\beta+2\gamma}\right)\Phi_D\psi}\right] \quad \text{(Eq. 4.1.20)}$$

$$\psi = 1+\left(\frac{1-\Phi_M}{{\Phi_M}^2}\right)\Phi_D \quad \text{(Eq. 4.1.21)}$$

Φ_M takes the same values as reported in Table 4.1.1.

The Lewis Nielsen model was initially presented for calculating elastic modulus of particulate composites (Nielsen, 1974) and can be extended to permeability (Pal, 2008) in the form:

$$P = P_C\frac{1+2\left(\frac{\lambda_{dc}-1}{\lambda_{dc}+2}\right)\Phi}{1-\left(\frac{\lambda_{dc}-1}{\lambda_{dc}+2}\right)\Phi\psi} \quad \text{(Eq. 4.1.22)}$$

where λ_{dc} is the permeability ratio of dispersed and continuous phase:

$$\lambda_{dc} = \frac{P_D}{P_C} \quad \text{(Eq. 4.1.23)}$$

and ψ is calculated with Eq. 4.1.21:

A generalized equation for Lewis Nielsen model considering shapes and orientations of the particles in dispersed phase, which can be applicable for all filled polymeric systems (Prasad *et al.*, 2021), is written as:

$$P = P_C\left(\frac{1+AB\Phi_D}{1-B\psi\Phi_D}\right) \quad \text{(Eq. 4.1.24)}$$

$$A = k_E - 1 \quad \text{(Eq. 4.1.25)}$$

$$B = \frac{\frac{P_D}{P_C}-1}{\frac{P_D}{P_C}+A} \quad \text{(Eq. 4.1.26)}$$

where k_E is the generalized Einstein coefficient, and A (Table 4.1.2) is a parameter considering the shape and orientation of dispersed phase (Nielsen, 1974).

Table 4.1.2 A values for different dispersed phase shapes (Nielsen, 1974).

Shape of dispersed phase	A
Spheres	1.5
Aggregated Spheres	2.5
Random rods, $\alpha = 2$	1.58
Random rods, $\alpha = 4$	2.08
Random rods, $\alpha = 6$	2.8
Random rods, $\alpha = 10$	4.93
Random rods, $\alpha = 15$	8.38
Fibres parallel to gas flow	2D/L
Fibres perpendicular to gas flow	0.5

Finally, Table 4.1.3 shows the summary of the existing models with their descriptions and characteristics.

Table 4.1.3 Summary of existing models.

Models	Characteristics
Additive (rule of mixtures)	Dispersed phase and matrix are independent where they do not interact with each other, inter-particle distances are large.
Laminate (reciprocal)	Used for Multi-layer films/laminates. Layers are homogeneous and defect free, accurate thicknesses of layers are required.
Logarithmic model	Another version of additive model.
Maxwell	Originally developed for electrical conductivity of composites.
	Applied for low filler volume fraction. ($0 < \Phi < 0.2$).
	Size, shapes of particles are not considered.
	Explicit relation which is easy to solve.
Chiew and Glandt	Originally applied for composite thermal conductivity.
	Shape and distribution of dispersed particles are considered.
	Interactions between phases and between particles are considered.
	Relation between permeability of dispersed phase and matrix is considered.
	Explicit relation.
Bruggeman	Used originally for composite dielectric constant.
	Broader range of Φ compared with Maxwell model.
	Shapes, size of particles are ignored.
	Implicit relation which needs numerical solving
Pal	Developed originally for thermal conductivity of composites.
	Broad range of Φ, $0 < \Phi < \Phi_M$.
	Take into account the effects of shapes, size of particles.
	Consider defects of interfacial layer between filler and matrix.
	Implicit relation.

Felske	Originally created for composite thermal conductivity. Applied just for low volume fraction of dispersed phase. The interfacial layer between dispersed phase and matrix is considered. Explicit relation.
Lewis Nielsen	Applied originally for elastic modulus of composites. Low range of Φ. Shapes and particle orientations are taken into account. Explicit relation. Being applied for all polymeric composites.

4.2 Description of the model used in this work

Exploiting the analogy between mass transfer and heat transfer in this work, a model based on the simulation of heat transfer through a model cell in which with filler particles are present was used to predict the oxygen permeability of a composite material with cellulosic filler.

The model used ANSYS Fluent software to solve a heat transfer problem. ANSYS Fluent is a computational fluid dynamic software, used for predicting fluid flow and heat transfer. We take advantage of the analogy between heat and mass transfer, based on the fact that the same set of equations describes both the diffusion of a gas and the conduction of heat in a solid. Consequently, the ratio of the heat flow rates obtained from the simulation with varying volume fraction of cellulose fillers particles to the heat flow rate in the absence of particles is equal to the ratio of the mass flow rates in the same conditions, and thus to the ratio of the oxygen permeability of composites with different volume fraction of cellulose fillers particles to the permeability of polymer matrix with no particle:

$$\frac{\dot{Q}_{\text{with cellulose particles}}}{\dot{Q}_{\text{without cellulose particle}}} = \frac{P_{\text{with cellulose particles}}}{P_{\text{without cellulose particle}}}$$

The model simulates the heat transfer in a model cell having the shape of a rectangular cuboid, in which a heat flow rate is determined by the temperature difference applied to two opposite faces of the cuboid. The temperature difference and the dimensions of the cuboid are kept constant, while the volume fraction of particles inside the cuboid, their spatial distribution and their aspect ratio is varied. Symmetric boundary conditions are prescribed at the lateral walls of the cuboid. This is equivalent to assume that the system is formed by infinitely many lateral replicates of the cuboid. The heat flow rate of the cuboid in the absence of particles is calculated by the equation:

$$\dot{Q}_{\text{without cellulose particle}} = k\frac{\Delta T}{\delta}A$$

in which:

- k is thermal conductivity of the solid, which was set to k = 0.0246 (W/m.K).
- ΔT is the temperature difference between two opposite faces of the cuboid.
- δ is the width of cuboid, in the direction of the heat flow.
- A is surface area of the faces of the cuboid to which the temperature difference is applied

The model is applied to the results of the study of Galland et al. (2014), reporting the permeability of nanocomposites made of a hyperbranched polymer matrix filled with 10 vol%, 40 vol% and 60 %vol of nanocellulose. This study was chosen for testing the model as it reported permeability measurements for a wide range of cellulose particle volume fractions.

The dimensions of the model cuboid were set at 6.6 mm, 7 mm, 0.35 mm along the x, y, z-axis. The dimensions of the cuboid were designed in order to be able to fit a layer of cylindrical particles in the x,y plane (Figure 4.2.4), representing a layer of cellulose particles idealized as having a rod-like shape.

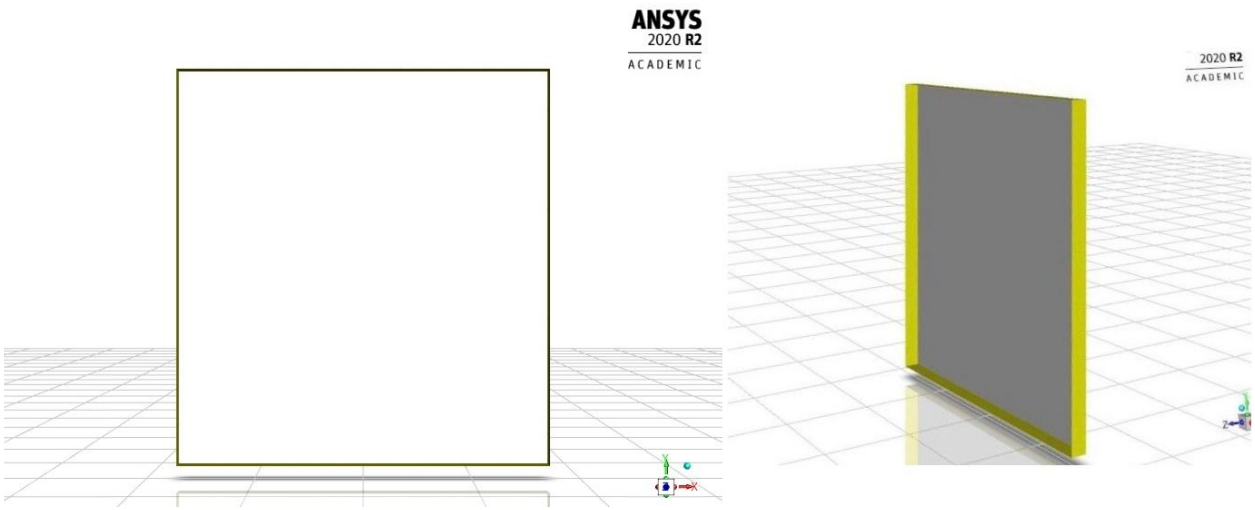

Figure 4.2.1 Geometry of the cuboid.

In a first set of simulations, the particles were represented by cylinders with dimension of 0.312 mm in diameter and 6.25 mm in length, thus having an aspect ratio of length to diameter equal to 40. Therefore:

- Volume of the cuboid is: V = 6.6 x 7 x 0.35 = 16 mm^3.
- Volume of one particle is: V = π x 0.156^2 x 6.25 = 0.48 mm^3.

All particles are assumed to have the same shape and size, to lie equidistantly on the xy-plane which is perpendicular to heat transfer direction (z-axis). They are simulated as non-conducting solid cylinders. In the heat-mass transfer analogy this setting corresponds to non-permeable particles. The number of particles inside the cuboid is calculated in order to obtain the same volume fractions of filler as in the composites studied by Galland *et al.* (2014). As such in this simulation three scenarios will be tested: Scenario 1 with particles volume fraction of 10 vol%; Scenario 2 with particles volume fraction of 40 vol% ; Scenario 3 with particles volume fraction of 60 vol%.

The temperature difference can be set arbitrarily, since the results of the simulation focus on the ratios of heat flow rate with the same temperature difference in all the scenarios. In this simulation, temperature of the front surface of the cuboid is set at 400 ^oC and temperature of

the back surface is set at 300 °C. The total heat flow rate through an area surface of 6.6 mm x 7 mm is obtained by:

$$\dot{Q} = 0.0246 \times \frac{100}{0.35 \times 10^{-3}} \times [(6.6 \times 10^{-3}) \times (7 \times 10^{-3})] = 0.32472 \text{ (W)}.$$

Scenario 1: Since the volume of cuboid is 16 mm^3 and the volume of one particle is 0.48 mm^3, a volume fraction of particles of 10% is obtained when 3 particles are inside the cuboid, as represented in Figure 4.2.2.

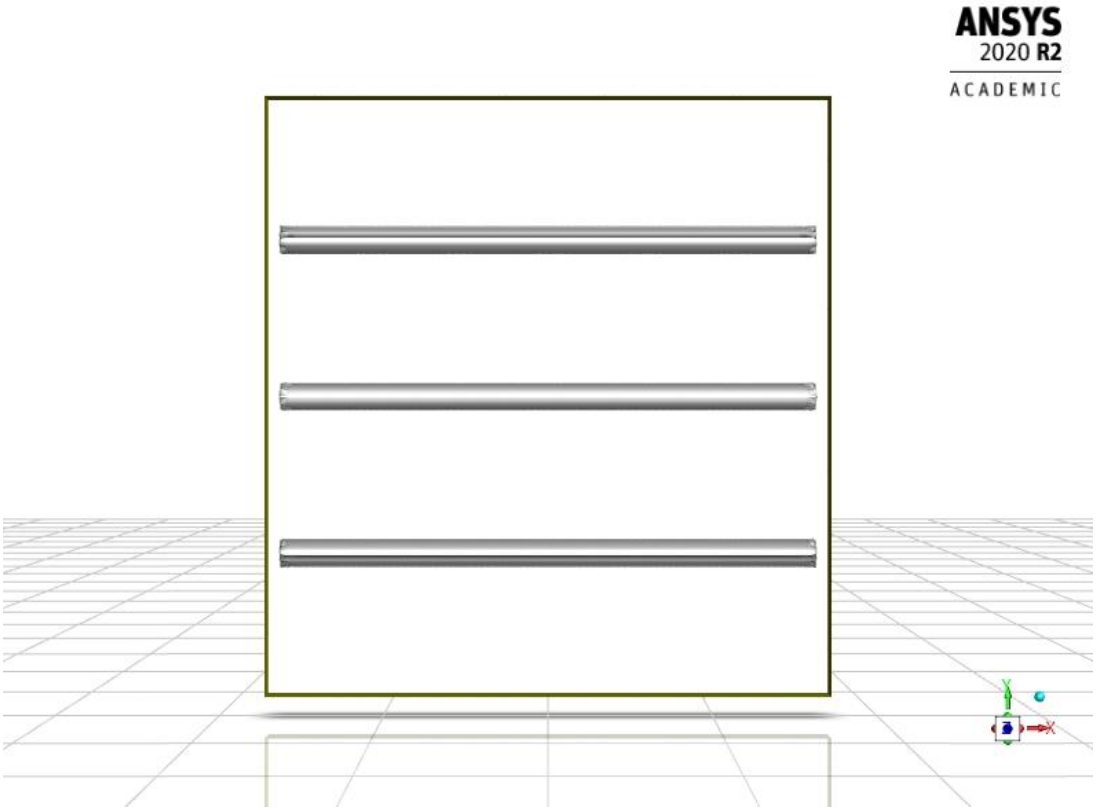

Figure 4.2.2 Model cell containing 10 vol% particles.

Running the simulation, a total heat flow rate of 0.288 (W) is obtained. Therefore, the ratio of $\dot{Q}$ with 10 vol% particles to $\dot{Q}$ without particle is 0.288 / 0.32472 = 0.89. According to this result, as the permeability of the unfilled polymer was 37 ($cc.\mu m.m^{-2}.day^{-1}.kPa^{-1}$), the calculated permeability for a composite with 10 vol% of cellulose would be 0.89 x 37 = 32.93 ($cc.\mu m.m^{-2}.day^{-1}.kPa^{-1}$).

Scenario 2: With 40 vol% of particles, the number of particles inside the cuboid increases to 13 (Figure 4.2.3).

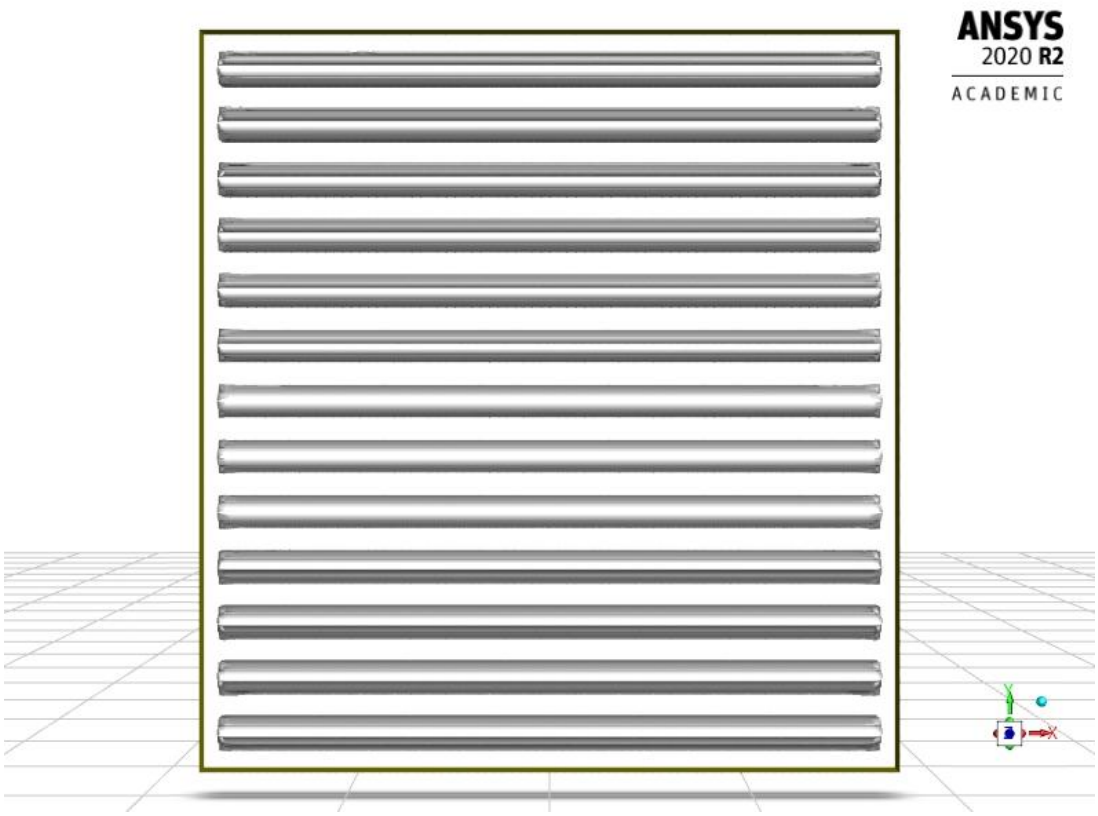

Figure 4.2.3 Model cell containing 40 vol% particles.

The recorded total surface heat flow rate is 0.1613 (W) and the ratio of $\dot{Q}$ with 40 vol% particles to $\dot{Q}$ without particle is 0.1613 / 0.32472 = 0.5. Permeability for a composite with 40 vol% of cellulose is calculated: 0.5 x 37 = 18.38 (cc.µm.m^{-2}.day^{-1} .kPa^{-1}).

Scenario 3: When the particle volume fraction increases to 60 vol%, 20 particles are present.

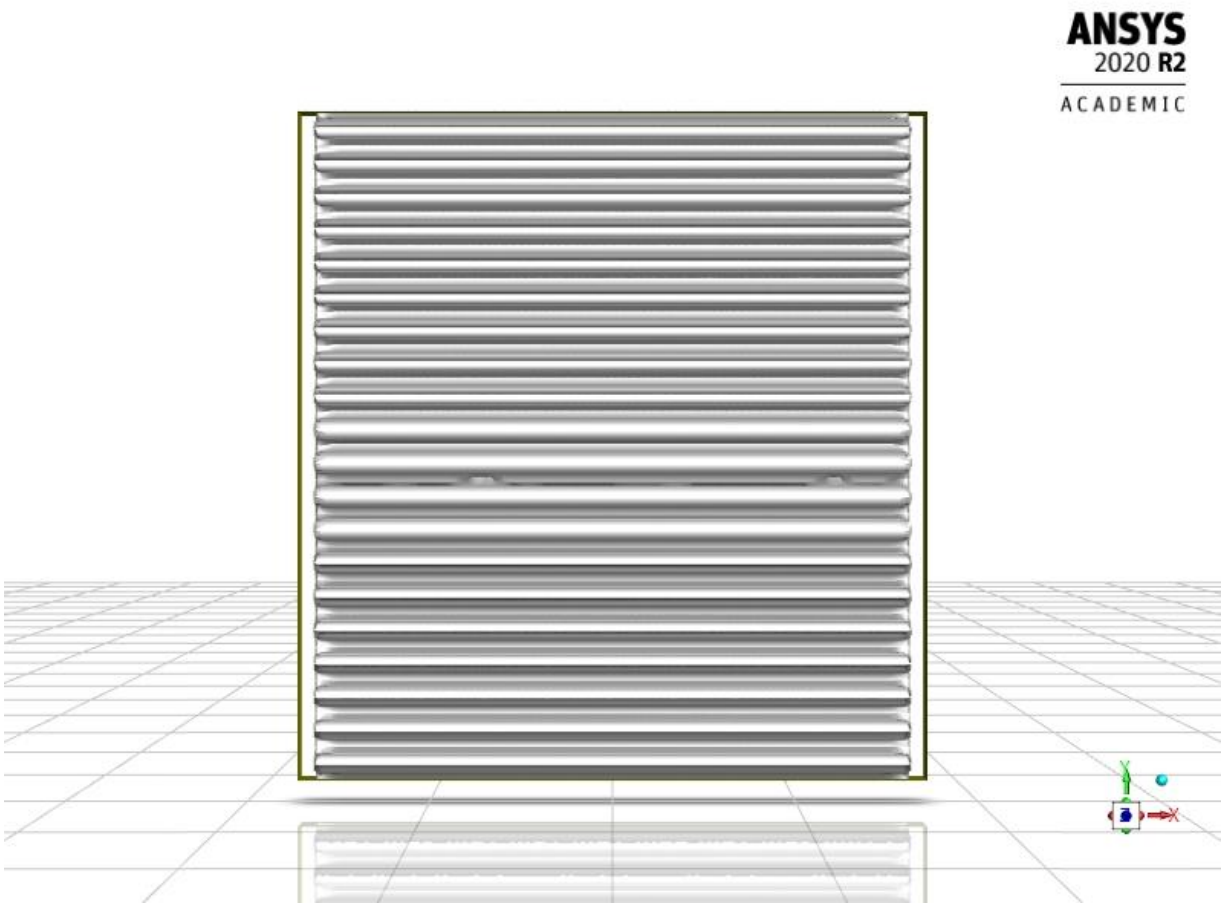

Figure 4.2.4 Scheme of 60 vol% particles.

From the simulation, with 60 vol% of particles, the total surface heat flow rate is 0.018 (W) and the ratio of $\dot{Q}$ with 60 vol% particles to $\dot{Q}$ without particles is 0.018 / 0.32472 = 0.055. The calculated permeability for a composite with 60 vol% of cellulose would be: 0.055 x 37 = 2.05 ($cc.\mu m.m^{-2}.day^{-1}.kPa^{-1}$).

From the three results obtained with the simulation software, when the number (i.e. the volume fraction) of particles inside the cuboid increases, the total surface heat flow rate decreases, and therefore also the permeability decreases.

Moreover, another scenario was tested to calculate the effect of a different special distribution of the particles, keeping the same dimensions for the cuboid and the particles. Based on scenario 2, with 40 vol% of particles, a simulation was conducted with no space between particles (Figure 4.2.5). Running the simulation, the total surface heat flow rate reaches 0.148 (W) and the ratio of $\dot{Q}$ with 40 vol% particles to $\dot{Q}$ without particles is 0.148 / 0.32472 = 0.46, which decreases compared to scenario 2, thus a lower permeability, equal to 0.46 x 37 = 16.86 ($cc.\mu m.m^{-2}.day^{-1}.kPa^{-1}$) is calculated for this configuration.

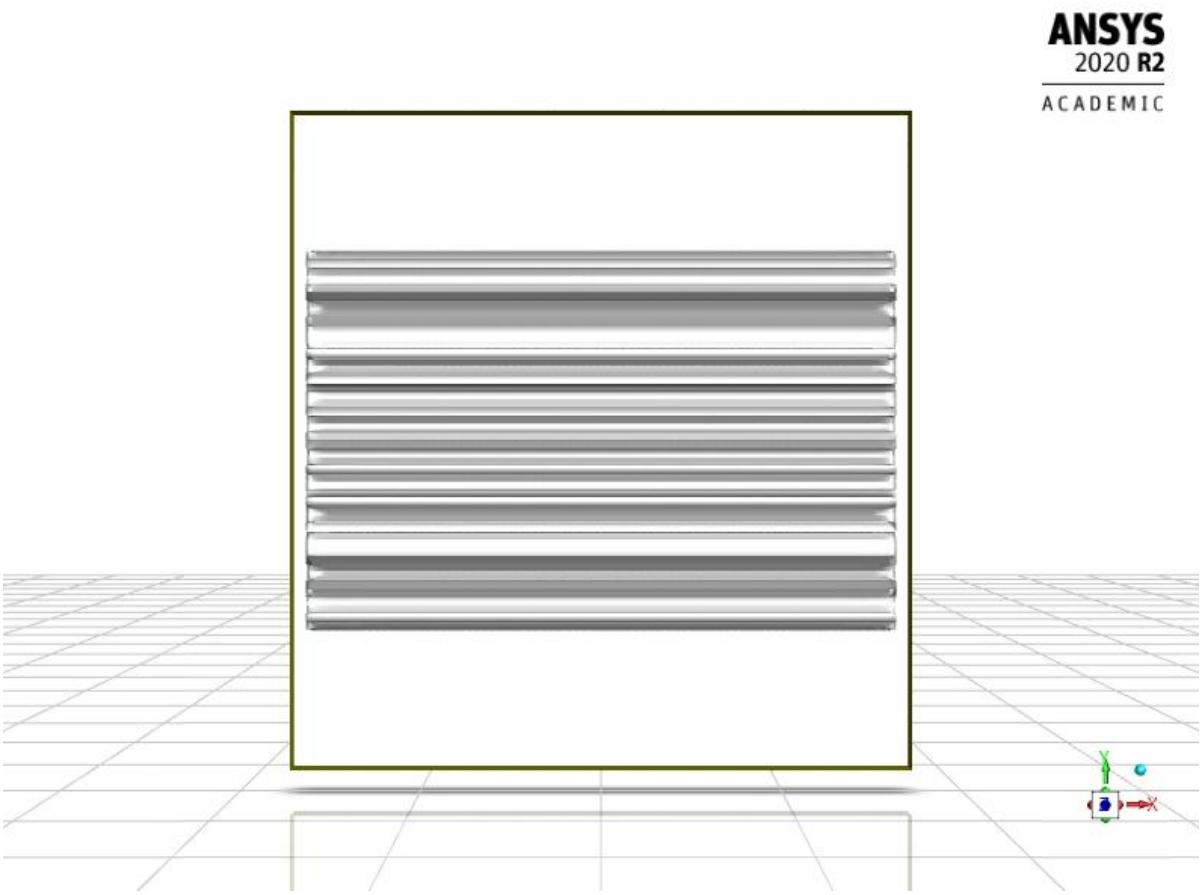

Figure 4.2.5 Scheme of 40 vol% particles where particles are in contact.

To test the effect of aspect ratio of particles on the permeability, another simulation was run with particles having an aspect ratio of 30. The dimensions of the particles were thus set at 0.344 mm in diameter and 5.162 mm in length. An increased total surface heat flow rate was observed, in particular, $\dot{Q} = 0.18$ (W). The permeability value calculated in this case was 20.5 ($cc.\mu m.m^{-2}.day^{-1}.kPa^{-1}$).

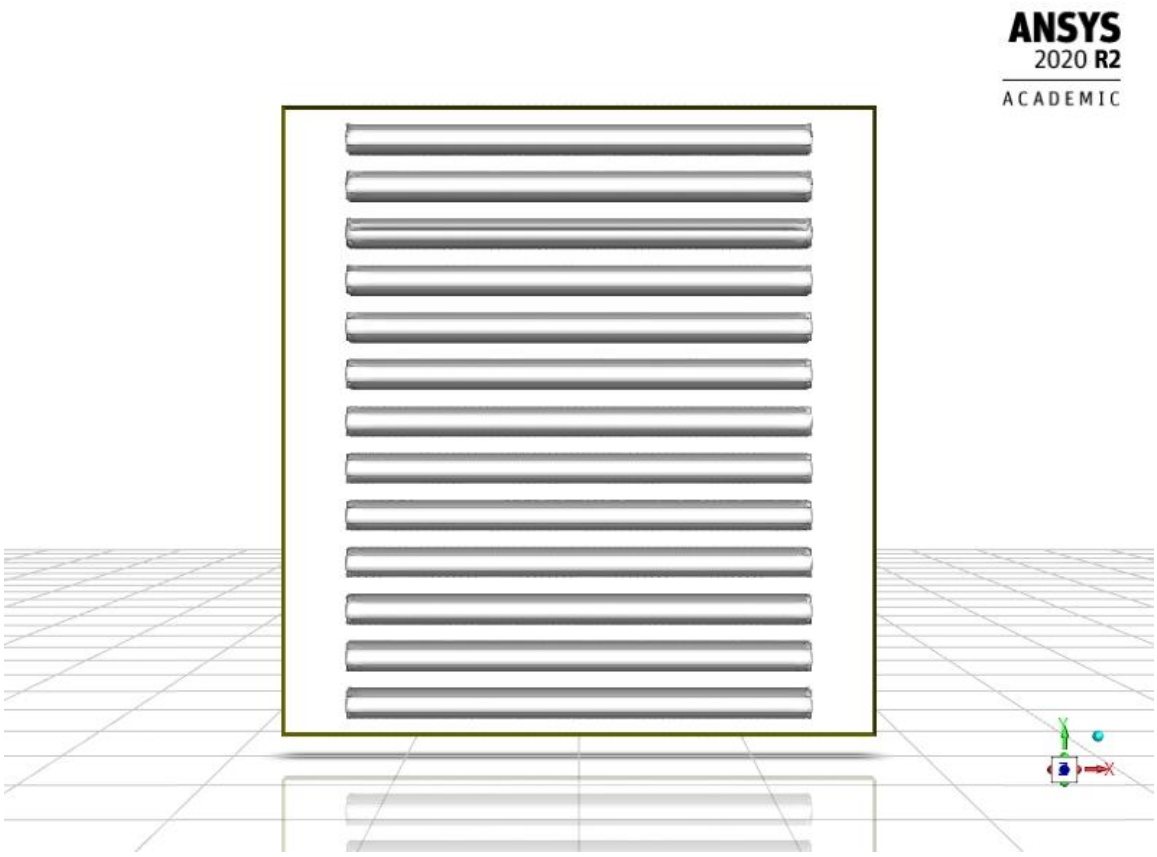

Figure 4.2.7 Scheme of 40 vol% particles with lower aspect ratio.

4.3 Discussion

The simulation shows the effect of the volume fraction of particles presented in the cuboid on the total surface heat flow rate, and thus on the permeability calculated by utilizing the analogy between heat and mass transfer. The permeability decreases from 37 (cc.µm.m^{-2}.day^{-1} .kPa^{-1}) with no particles to 32.93 (cc.µm.m^{-2}.day^{-1} .kPa^{-1}) when 10 vol% of particles is present. When the volume fraction of particles increases to 40 vol%, permeability of the composite keeps decreasing and reaches 18.38 (cc.µm.m^{-2}.day^{-1} .kPa^{-1}). Increasing the volume fraction of particle to 60% resulting in permeability of 2.05 (cc.µm.m^{-2}.day^{-1} .kPa^{-1}).

This observation is in line with experimental results in various literatures for the permeability of composites where, in the presence of fillers, permeability decreases with increasing filler volume fraction. As reported e.g. by Galland *et al.* (2014), Jung *et al.* (2020), Djordjevic *et al.* (2016), Sanchez-Garcia and Lagaron (2010. However, in the simulation, the permeability with 60 vol% particles decreased sharply compared to the scenarios with 10 vol% and 40 vol%. On the other hand, in the experiment of Galland *et al.* (2014), oxygen permeability with 60 vol% cellulosic filler only reduced slightly compared to permeability with 10 vol% and 40 vol% cellulosic filler, as illustrated on Figure 4.2.8. This result may be attributed to the possible agglomeration of cellulose or to an increased presence of defects at the cellulose-polymer interface when the volume fraction increases, which are not taken into account in the simulation.

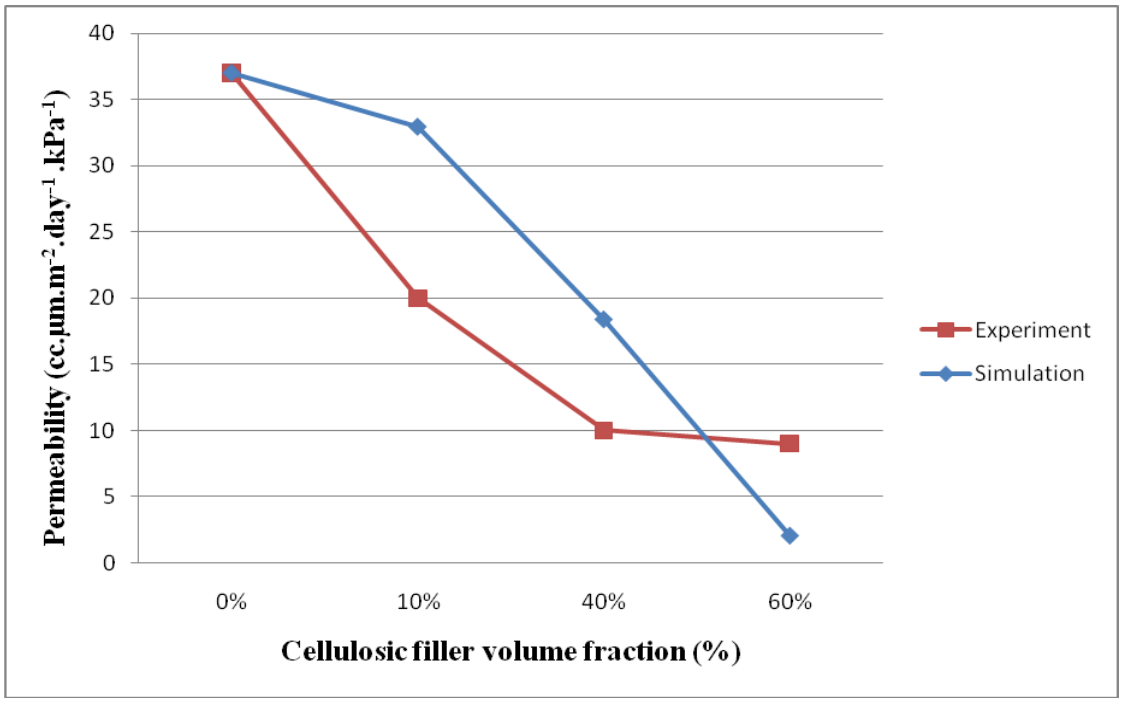

Figure 4.2.8 The experimental and simulated values of permeability versus the volume fraction of cellulose.

The effect of particle spatial arrangement was tested with the simulation. In particular, when particles lied adjacently without any space between, surface heat flow rate was lowered from 0.1613 to 0.148 (W), thus permeability was found to decrease. This effect contrasts with experimental results from Jung *et al.* (2020), where the agglomeration of nanocellulose increased the oxygen permeability of composites by creating chink and crack on the interface between filler and matrix (Jung *et al.*, 2020). On the other hand, the configuration could look like a platelet, which is more efficient than a cylinder at improving barrier properties as reducing the permeability (Wolf *et al.*, 2018).

In addition, the effect of particles aspect ratio on permeability was further investigated. When the aspect ratio length/diameter of particles decreased from 40 to 30, the total surface heat flow rate increased from 0.1613 to 0.18 (W), thus permeability increased, as expected.

The effects of temperature and humidity level of the system were not considered in the simulation. In literature experiments, oxygen permeability value of composite increased when the relative humidity increased (Galland *et al.*, 2014). The simulation did not take into account the effects of plasticizers as well as the effect of nanocellulose on the crystalline and amorphous regions of polymers which affect the barrier properties (Jung *et al.*, 2020). For future work, the simulation can be further improved by designing particles closer to the shapes and aspect ratios of the particles and to the actual spatial arrangement of cellulosic fillers.

5. Conclusions

This manuscript presents a review on cellulosic fillers and composites with nanocellulose, and collects data about the oxygen permeability of these materials taking into account different parameters, such as volume fraction and aspect ratio of cellulosic fillers.

A simulation was performed with ANSYS software for predicting the transport of gas in the composite films, and therefore the permeability, using the analogy between heat and mass transfer to solve Fick's equation. The simulation studied the relationship between the heat flow rate and the volume fraction of cylindrical particles inside a cuboid to predict the relationship between permeability and volume fraction of cellulosic fillers in a polymeric matrix. Literature data (Galland *et al.* 2014) were used to test the model.

The results of preliminary simulations found that the permeability decreased with increased volume fraction of the filler, as expected based on research works of Galland *et al.* (2014), Jung *et al.* (2020), Djordjevic *et al.* (2016), Sanchez-Garcia and Lagaron (2010). However, compared to the results of Galland *et al.* (2014), at higher particles content, the expected permeability is lower than the experimental results suggesting that at high volume fractions agglomeration of nanocellulose or defects at the matrix filler interface may affect the results. In addition, the spatial distribution and the aspect ratio of particles were observed to influence permeability. Particularly, in agreement with experimental measurements, a decrease of aspect ratio results in an increase of permeability.

References

ASTM D1434-82(2015)e1, Standard Test Method for Determining Gas Permeability Characteristics of Plastic Film and Sheeting, *ASTM International*, West Conshohocken, PA, 2015, www.astm.org. [DOI: 10.1520/D1434-82R15E01]

ASTM D3985-17, Standard Test Method for Oxygen Gas Transmission Rate Through Plastic Film and Sheeting Using a Coulometric Sensor. *ASTM International*, West Conshohocken, PA, 2017, www.astm.org. [DOI: 10.1520/D3985-17]

ASTM F1307-20, Standard Test Method for Oxygen Transmission Rate Through Dry Packages Using a Coulometric Sensor. *ASTM International*, West Conshohocken, PA, 2020, www.astm.org. [DOI: 10.1520/F1307-20]

ASTM F1927-20, Standard Test Method for Determination of Oxygen Gas Transmission Rate, Permeability and Permeance at Controlled Relative Humidity Through Barrier Materials Using a Coulometric Detector. *ASTM International*, West Conshohocken, PA, 2020, www.astm.org. [DOI: 10.1520/F1927-20]

ASTM F2622-20, Standard Test Method for Oxygen Gas Transmission Rate Through Plastic Film and Sheeting Using Various Sensors, *ASTM International*, West Conshohocken, PA, 2020, www.astm.org. [DOI: 10.1520/F2622-20]

ASTM F3136-15, Standard Test Method for Oxygen Gas Transmission Rate through Plastic Film and Sheeting using a Dynamic Accumulation Method. *ASTM International*, West Conshohocken, PA, 2015, www.astm.org. [DOI: 10.1520/F3136-15]

Azwa Z.N. , Yousif B.F., Manalo A.C. , Karunasena W., 2012, A review on the degradability of polymeric composites based on natural fibres. *Materials and Design* 47 (2013) 424–442. [DOI: 10.1016/j.matdes.2012.11.025]

Bledzki A.K., Gassan J., 1998, Composites reinforced with cellulose based fibres. *Prog. Polym. Sci.* 24 (1999) 221–274. [PII: S0079-6700(98)00018-5]

Böttcher C. J. F., 2010, The Dielectric Constant of Crystalline Powders. *Recl. Trav. Chim. Pays Bas* 2010, 64, 47–51. [DOI: 10.1002/recl.19450640205]

Chaker A., Mutje P., Vilaseca F., Boufi S., 2013, Reinforcing Potential of Nanofibrillated Cellulose From Nonwoody Plants. *Polymer composites*, Volume 34, Issue 12, December 2013, Pages 1999-2007. [DOI: 10.1002/pc.22607]

Chakrabarty A., Teramoto Y., 2018, Recent Advances in Nanocellulose Composites with Polymers: A Guide for Choosing Partners and How to Incorporate Them. *Polymers* 2018, 10(5), 517. [DOI: 10.3390/polym10050517]

Chaos A., Sangroniz A., Gonzalez A., Iriarte M., Sarasu J.R., Río J.D., Etxeberria A., 2018, Tributyl citrate as an effective plasticizer for biodegradable polymers: effect of plasticizer on free volume and transport and mechanical properties. *Polym Int* 2019; 68: 125–133. [DOI 10.1002/pi.5705]

Chiew Y.C., Glandt E.D., 1982, The effect of structure on the conductivity of a dispersion. J. Colloid Interface Sci. 94 (1983) 90–104. [DOI: 10.1016/0021-9797(83)90238-2]

Chung T.S., Jiang L.Y., Li Y., Kulprathipanja S., 2007, Mixed matrix membranes (MMMs) comprising organic polymers with dispersed inorganic fillers for gas separation. *Progress in Polymer Science* Volume 32, Issue 4, Pages 483-507. [DOI: 10.1016/j.progpolymsci.2007.01.008]

Coelho C.C.S., Michelin M., Cerqueira M.A., Gonçalves C., Tonon R.V., Pastrana L.M.,

Freitas-Silva O., Vicente A.A., Cabral L.M.C., Teixeira J.A., 2018, Cellulose nanocrystals from grape pomace: Production, properties and cytotoxicity assessment. *Carbohydrate Polymers*, Volume 192, 15 July 2018, Pages 327-336. [DOI: 10.1016/j.carbpol.2018.03.023]

DeLassus P., 2002, Barrier Polymers. *Kirk-Othmer Encyclopedia of Chemical Technology*, Vol 3, page 375-407. [DOI: 10.1002/0471238961.0201181804051201.a01.pub2]

Djordjevic N., Marinkovic A., Nikolic J., Drmanić S.Z., Rančić M., Brković D.V., Uskokovic P., 2016, A study of the barrier properties of polyethylene coated with nanocellulose/magnetite composite film. *Journal of the Serbian Chemical Society* 81 (0) 1–13 (2016) [DOI: 10.2298/JSC151217019D]

Dufresne A., 2018, Cellulose nanomaterials as green nanoreinforcements for polymer nanocomposites. *Phil. Trans. R. Soc. A* 376: 20170040. [DOI: 10.1098/rsta.2017.0040]

Feldman D., 2015, Cellulose Nanocomposites. *Journal of Macromolecular Science*, Part A, 52:4, 322-329, [DOI: 10.1080/10601325.2015.1007279]

Ferrer A., Pal L., Hubbe M., 2015, Nanocellulose in packaging: Advances in barrier layer technologies. *Industrial Crops and Products* 95 (2017) 574–582. [DOI: 10.1016/j.indcrop.2016.11.012]

Galland S., Leterrier Y., Nardi T., Plummer C.J.G., Månson J.A.E., Berglund L.A., 2014, UV-Cured Cellulose Nanofiber Composites with Moisture Durable Oxygen Barrier Properties. *J. APPL. POLYM. SCI.* 2014. [DOI: 10.1002/APP.40604]

Gangurde N., Sayyed R.Z., 2012, Poly-β-hydroxybutyrate (PhB): a Biodegradable Polymer of microbial origin. *Natural Polymers, Biopolymers, Biomaterials, and Their Composites, Blends, and IPNs*. [ISBN: 9780429096839]

Gonzo E.E., Parentis M.L., Gottifredi J.C., 2005, Estimating models for predicting effective permeability of mixed matrix membranes. *Journal of Membrane Science* 277 (2006) 46–54. [DOI:10.1016/j.memsci.2005.10.007]

Habibi Y., Lucia L.A., Rojas O.J., 2010, Cellulose Nanocrystals: Chemistry, Self-Assembly, and Applications. *Chem. Rev.* 2010, 110, 3479–3500.

Hashemifard S.A., Ismail A.F., Matsuura T., 2009, Prediction of gas permeability in mixed matrix membranes using theoretical models. *Journal of Membrane Science* 347 (2010) 53–61. [DOI:10.1016/j.memsci.2009.10.005]

Hatch K.M., Hlavatá J., Paulett K., Liavitskaya T., Vyazovkin S., Stanishevsky A.V., 2019, Nanocrystalline Cellulose/Polyvinylpyrrolidone Fibrous Composites Prepared by Electrospinning and Thermal Crosslinking. *International Journal of Polymer Science*, Volume 2019, Article ID 7103936, 12 pages. [DOI: 10.1155/2019/7103936]

Hatton F.L., Malmström E., Carlmark A., 2015, Tailor-made copolymers for the adsorption to cellulosic surfaces. *European Polymer Journal*, Volume 65, April 2015, Pages 325-339. [DOI: 10.1016/j.eurpolymj.2015.01.026]

Hinterstoisser B., Åkerholm M., Salmén L., 2003, Load Distribution in Native Cellulose. *Biomacromolecules* 2003, 4, 1232-1237.

Huang C.H., Wu J.S., Huang C.C., 2004, Predicting the permeability and tensile behavior of high density polyethylene/tie/polyamide 6 three-layer films. *Polym Int* 53, 2099–2106 (2004) [DOI: 10.1002/pi.1634]

Hubbe M.A., Rojas O.J., Lucia L.A., Sain M., 2008, Cellulosic nanocomposites: A review.

BioResources 3(3), 929-980. http://www.lib.ncsu.edu/resolver/1840.2/1843

Ishtiaque S., Naz S., Ahmed J., Faruqui A., 2018, Barrier Properties Analysis of Polyethylene Terephthalate Films (PET) Coated with Natural Polyphenolic and Gelatin Mixture (PGM). *Defect and Diffusion Forum*, 382, 38–43. [DOI: 10.4028/www.scientific.net/ddf.382.38]

Joseph B., Sagarika V K, Sabu C., Kalarikkal N., Thomas S., 2020, Cellulose nanocomposites: Fabrication and biomedical applications. *Journal of Bioresources and Bioproducts*, Vol 5, Issue 4, November 2020, Pages 223-237. [DOI: 10.1016/j.jobab.2020.10.001]

Jozala A.F., de Lencastre-Novaes L.C., Lopes A.M., Santos-Ebinuma V.D.C., Mazzola P.G., Pessoa-Jr A., Grotto D., Gerenutti M., Chaud M.V., 2016, Bacterial nanocellulose production and application: a 10-year overview. *Appl Microbiol Biotechnol* (2016) 100:2063–2072 [DOI 10.1007/s00253-015-7243-4]

Jozala A.F., Pértile R.A.N., dos Santos C.A., de Carvalho Santos-Ebinuma V., Seckler M.M., Gama F.M., Adalberto Pessoa Jr., 2014, Bacterial cellulose production by Gluconacetobacter xylinus by employing alternative culture media. *Appl Microbiol Biotechnol* 99, 1181–1190 (2015). [DOI: 10.1007/s00253-014-6232-3]

Jung B.N., Jung H.W., Kang D.H., Kim G.H., Lee M., Shim J.K., Hwang S.W., 2020, The fabrication of flexible and oxygen barrier cellulose nanofiber/polylactic acid nanocomposites using cosolvent system. *J Appl Polym Sci.* 2020;137:e49536. [DOI: 10.1002/app.49536]

Kargarzadeh H., Mariano M., Huang J., Lin N., Ahmad I., Dufresne A., Thomas S., 2017, Recent developments on nanocellulose reinforced polymer nanocomposites: A review. *Polymer* 132 (2017) 368-393. [DOI: 10.1016/j.polymer.2017.09.043]

Keller P.E., Kouzes R., 2017, Water Vapor Permeation in Plastics. [PNNL-26070] [DOI: 10.2172/1411940]

Klemm D., Cranston E.D., Fischer D., Gama M., Kedzior S.A., Kralisch D., Kramer F., Kondo T., Lindström T., Nietzsche S., Petzold-Welcke K., Rauchfuß F., 2018, Nanocellulose as a natural source for groundbreaking applications in materials science: Today's state. *Materials Today*, Volume 21, Issue 7, September 2018, Pages 720-748. [DOI: 10.1016/j.mattod.2018.02.001]

Klemm D., Heublein B., Fink H.P., Bohn A., 2005, Cellulose: Fascinating Biopolymer and Sustainable Raw Material. *Angew. Chem. Int. Ed.* 2005, 44, 3358 – 3393. [DOI: 10.1002/anie.200460587]

Klemm D., Kramer F., Moritz S., Lindstrom T., Ankerfors M., Gray D., Dorris A., 2011, Nanocelluloses: A New Family of Nature-Based Materials. *Angew. Chem. Int. Ed.* 2011, 50, 5438 – 5466. [DOI: 10.1002/anie.201001273]

Krehalon, 2020, PVDC: Why the fresh meat packaging industry can survive without it? Available online at https://www.krehalon.com/en/articles/pvdc-barrier-in-fresh-meat-packaging/

Lagaron J.M., Catalá R., Gavara R., 2004, Structural characteristics defining high barrier properties in polymeric materials, *Materials Science and Technology*, Vol 20, 1, page 1-7. [DOI: 10.1179/026708304225010442] [DOI: 10.1179/026708304225010442]

Lavanya D., Dixit M., Prudhvi Kanth Raavi, Krishna V., 2011, Sources of cellulose and their applications - A review. *IJDFR* volume 2 Issue 6. [ISSN 2229-5054]

Lin D., Liu Z., Shen R., Chen S., Yang X., 2020, Bacterial cellulose in food industry: Current research and future prospects. *International Journal of Biological Macromolecules* 158 (2020) 1007–1019. [DOI: 10.1016/j.ijbiomac.2020.04.230]

Lin N., Dufresne A., 2014, Nanocellulose in biomedicine: Current status and future prospect. *European Polymer Journal*, Volume 59, October 2014, Pages 302-325. [DOI: 10.1016/j.eurpolymj.2014.07.025]

Liu W., Du H., Zhang M., Liu K., Liu H., Xie H., Zhang X., Si C., 2020, Bacterial Cellulose-Based Composite Scaffolds for Biomedical Applications: A Review. *ACS Sustainable Chemistry & Engineering* 2020 8 (20), 7536-7562 [DOI: 10.1021/acssuschemeng.0c00125]

Lu Y., Tekinalp H. L.; Peter W. H., Eberle C., Naskar A. K., Ozcan S., 2014, Nanocellulose in Polymer Composites and Biomedical Applications. *Tappi J.* 2014, 13, 47−54. [DOI: 10.32964/tj13.6.47]

Maes C., Luyten W., Herremans G., Peeters R., Carleer R., Buntinx M., 2018, Recent Updates on the Barrier Properties of Ethylene Vinyl Alcohol Copolymer (EVOH): A Review. *Polymer Reviews*, 2018, Vol. 58, No. 2, 209–246. [DOI: 10.1080/15583724.2017.1394323]

Mannan H. A., Mukhtar H., Murugesan T., Man Z., Bustam M.A., Shaharun M. S., Abu Bakar M. Z., 2017, Prediction of CO2 gas permeability behavior of ionic liquid–polymer membranes (ILPM). *J. APPL. POLYM. SCI.* Volume 134, Issue 17. [DOI: 10.1002/APP.44761]

Markets and Markets, 2018, Nanocellulose Market. Available online at https://www.marketsandmarkets.com/PressReleases/nanocellulose.asp

Marsh K., Bugusu B., 2007, Food Packaging—Roles, Materials, and Environmental Issues. *Journal of Food Science*, Volume 72, Issue 3, Pages R39-R55. [DOI: 10.1111/j.1750-3841.2007.00301.x]

Martínez-Sanz M., Lopez-Rubio A., Lagaron J.M., 2013, High-barrier coated bacterial cellulose nanowhiskers films with reduced moisture sensitivity. *Carbohydrate Polymers* 98 (2013) 1072– 1082. [DOI: 10.1016/j.carbpol.2013.07.020]

Matmatch, Thermoplastics vs. Thermosetting Polymers: Properties, Processing and Applications. Available online at https://matmatch.com/learn/material/thermoplastics-vs-thermosetting-polymers

Maxwell A.S., Roberts S.J., 2008, Review of Data on Gas Migration through Polymer Encapsulants. Report to NDA - Radioactive Waste Management Directorate. *SERCO/TAS/000500/001* – Issue 2

Mohammed L., Ansari M.N.M., Pua G., Jawaid M., Islam M.S., 2015, A Review on Natural Fiber Reinforced Polymer Composite and Its Applications. *International Journal of Polymer Science*. Volume 2015, Article ID 243947, 15 pages. [DOI: 10.1155/2015/243947]

Monteiro S.N., Lopes F.P.D., Barbosa A.P., Bevitori A.B., Da Silva I.L.A., Da Costa L.L., 2011, Natural Lignocellulosic Fibers as Engineering Materials—An Overview. *Metallurgical and materials transactions A*, Volume 42a, October 2011, 2963—2974. The Minerals, Metals & Materials Society and ASM International 2011. [DOI: 10.1007/s11661-011-0789-6]

Moon R.J., Schueneman G.T., Simonsen J., 2016, Overview of Cellulose Nanomaterials,

Their Capabilities and Applications. *JOM*, 68, 2383–2394 (2016). [DOI: 10.1007/s11837-016-2018-7]

Morán J.I., Alvarez V.A., Cyras V.P., Vázquez A., 2008, Extraction of cellulose and preparation of nanocellulose from sisal fibers. *Cellulose* 15, 149–159 (2008). [DOI: 10.1007/s10570-007-9145-9]

Mu R., Hong X., Ni Y., Li Y., Pang J., Wang Q., Xiao J., Zheng Y., 2019, Recent trends and applications of cellulose nanocrystals in food industry. *Trends in Food Science & Technology* 93 (2019) 136–144. [DOI: 10.1016/j.tifs.2019.09.013]

Nair S.S., Wang S., Hurley D.C., 2010, Nanoscale characterization of natural fibers and their composites using contact-resonance force microscopy. *Composites Part A: Applied Science and Manufacturing*, Volume 41, Issue 5, May 2010, Pages 624-631, [DOI: 10.1016/j.compositesa.2010.01.009]

Nair S.S., Zhu J.Y., Deng Y., Ragauskas A.J., 2014, High performance green barriers based on nanocellulose. *Sustainable Chemical Processes* 2014, 2:23. http://www.sustainablechemicalprocesses.com/content/2/1/23

Naz, S., Ali J.S., Zia M., 2019, Nanocellulose isolation characterization and applications: a journey from non-remedial to biomedical claims. *Bio-Design and Manufacturing* (2019) 2:187–212. [DOI: 10.1007/s42242-019-00049-4]

Nielsen L.E., The Thermal and Electrical Conductivity of Two-Phase Systems. *Ind. Eng. Chem. Fund.* 1974, 13, 17–20. [DOI: 10.1021/i160049a004]

Oksman K., Mathew A.P., Bondeson D., Kvien I., 2006, Manufacturing process of cellulose whiskers/polylactic acid nanocomposites. *Composites Science and Technology* 66 (2006) 2776–2784. [DOI: 10.1016/j.compscitech.2006.03.002]

Pal R., 2007, Permeation models for mixed matrix membranes. *Journal of Colloid and Interface Science* 317 (2008) 191–198. [DOI: 10.1016/j.jcis.2007.09.032]

Pandey J.K., Nakagaito A.N., Takagi H., 2012, Fabrication and applications of cellulose nanoparticle-based polymer composites. *Polymer engineering and science*. Volume 53, Issue 1, Pages 1-8. [DOI: 10.1002/pen.23242]

Peelman N., Ragaert P., Meulenaer B.D., Adons D., Peeters R., Cardon L., Impe F.V., Devlieghere F., 2013, Application of bioplastics for food packaging. *Trends in Food Science & Technology* 32 (2013) page 128-141. [DOI: 10.1016/j.tifs.2013.06.003]

Phanthong P., Reubroycharoen P., Hao X., Xu G., Abudula A., Guan G., 2018, Nanocellulose: Extraction and application. *Carbon Resources Conversion*, Volume 1, Issue 1, April 2018, Pages 32-43. [DOI: 10.1016/j.crcon.2018.05.004]

Prasad K., Nikzad M., Sbarski I., 2021, Modeling Permeability in Multi-Phase Polymer Composites: A Critical Review of Semi-Empirical Approaches. *Polymer Reviews*, Vol. 61, No. 1, Page 194-237. [DOI: 10.1080/15583724.2020.1743306]

Rashid E.S.A., Julkapli N.U., Yehye W.A., 2018, Nanocellulose reinforced as green agent in polymer matrix composites applications. *Polym Adv Technol.* Volume29, Issue6, June 2018, Pages 1531-1546. [DOI: 10.1002/pat.4264]

Raza Z.A., Aslam M., Azeem A., Maqsood H.S., 2019, Development and characterization of nano-crystalline cellulose incorporated poly(lactic acid) composite films. *Materialwiss. Werkstofftech.* 2019, 50, 64–73. [DOI: 10.1002/mawe.201800081]

Reese E.T., Mandels M., Weiss A.H., 2005, Cellulose as a novel energy source. *Advances in*

Biochemical Engineering, Volume 2 pp 181-200.

Rennie A.R., 1999, Thermoplastics and Thermosets. *Mechanical Properties and Testing of Polymers*. Polymer Science and Technology Series, vol 3. Springer, Dordrecht. [DOI: 10.1007/978-94-015-9231-4_53]

Rodionova G., Lenes M., Eriksen Ø., Gregersen Ø., 2010, Surface chemical modification of microfibrillated cellulose: improvement of barrier properties for packaging applications. *Cellulose*, February 2010. [DOI 10.1007/s10570-010-9474-y]

Rybak A., Rybak A., Sysel P., 2018, Modeling of Gas Permeation through Mixed-Matrix Membranes Using Novel Computer Application MOT. *Appl. Sci.* 2018, 8 (7), 1166. [DOI: 10.3390/app8071166]

Sanaeepur H., Amooghin A.E., Khademian E., Kargari A., Omidkhah M., 2017, Gas permeation modeling of mixed matrix membranes: Adsorption isotherms and permeability models. *Polymer Composites*, Volume 39, Issue 12, Pages 4560-4568. [DOI: 10.1002/pc.24564]

Sanchez-Garcia M.D., Lagaron J.M., 2010, On the use of plant cellulose nanowhiskers to enhance the barrier properties of polylactic acid. *Cellulose* (2010) 17:987–1004 [DOI: 10.1007/s10570-010-9430-x]

Sanjay M.R., Arpitha G.R., Naik L.L., Gopalakrisha K.,Yogesha B., 2016, Applications of Natural Fibers and Its Composites: An Overview. *Natural Resources*, 7, 108-114. [DOI: 10.4236/nr.2016.73011]

Sankhla S., Sardar H.H., Neogi S., 2020, Greener extraction of highly crystalline and thermally stable cellulose micro-fibers from sugarcane bagasse for cellulose nano-fibrils preparation. *Carbohydrate Polymers*, Volume 251, 1 January 2021, 117030, [DOI: 10.1016/j.carbpol.2020.117030]

Sekelik D.J., Stepanov E.V., Nazarenko S., Schiraldi D., Hiltner A., Baer E., 1999, Oxygen barrier properties of crystallized and talc-filled poly(ethylene terephthalate). *Journal of Polymer Science Part B: Polymer Physics*, Volume37, Issue8, 847–857, 1999 [DOI: 10.1002/(SICI)1099-0488(19990415)37:8<847::AID-POLB10>3.0.CO;2-3]

Sharma A., Thakur M., Bhattacharya M., Mandal T., Goswami S., 2019, Commercial application of cellulose nano-composites – A review. *Biotechnology Reports*, Volume 21, March 2019, e00316. [DOI: 10.1016/j.btre.2019.e00316]

Shen R., Xue S., Xu Y., Liu Q., Feng Z., Ren H., Zhai H., Kong F., 2020, Research Progress and Development Demand of Nanocellulose Reinforced Polymer Composites. *Polymers* 2020, 12, 2113; [DOI: 10.3390/polym12092113]

Shimekit B., Mukhtar H., Maitra S., 2010, Comparison of Predictive Models for Relative Permeability of CO2 in Matrimid-Carbon Molecular Sieve Mixed Matrix Membrane. *Journal of Applied Sciences*, 10: 1204-1211. [DOI: 10.3923/jas.2010.1204.1211]

Smithers, 2019, The Future of Global Packaging to 2024. Available online at https://www.smithers.com/en-gb/services/market-reports/packaging/future-of-global-packaging-to-2024

Strupinsky G., Brody A.L., 1998, A Twenty-Year Retrospective on Plastics: Oxygen Barrier Packaging Materials. *Polymers, laminations, & coatings conference*, Vol 1, 119-140. [ISBN 0898527198]

Sydow Z., Bieńczak K., 2019, The overview on the use of natural fibers reinforced

composites for food packaging. *Journal of Natural Fibers*, 16:8, 1189-1200. [DOI: 10.1080/15440478.2018.1455621]

Syverud K, Stenius P, 2008, Strength and barrier properties of MFC films. *Cellulose* 2009, 16:75-85. [DOI 10.1007/s10570-008-9244-2]

Textile School, 2019, Natural Cellulose Fibers – natures own fibers. Available online at https://www.textileschool.com/379/natural-cellulose-fibres-natures-own-fibres/

Thakur V.K., Thakur M.K., 2014, Processing and characterization of natural cellulose fibers/thermoset polymer composites. *Carbohydrate Polymers* 109 (2014) 102–117. [DOI: 10.1016/j.carbpol.2014.03.039]

Thomas B., Raj M.C., Athira K.B., Rubiyah M.H., Joy J., Moores A., Drisko G.L., Sanchez C., 2018, Nanocellulose, a Versatile Green Platform: From Biosources to Materials and Their Applications. *Chemical Reviews*. 2018 118 (24), 11575-11625. [DOI: 10.1021/acs.chemrev.7b00627]

Thyavihalli Girijappa Y.G., Mavinkere Rangappa S., Parameswaranpillai J., Siengchin S., 2019, Natural Fibers as Sustainable and Renewable Resource for Development of Eco-Friendly Composites: A Comprehensive Review. *Front. Mater.* 6:226. [DOI: 10.3389/fmats.2019.00226]

Trache D., 2018, Nanocellulose as a promising sustainable material for biomedical applications. *AIMS Materials Science* 2018, Volume 5, Issue 2: 201-205. [DOI: 10.3934/matersci.2018.2.201]

Trache D., Tarchoun A.F., Derradji M., Hamidon T.S., Masruchin N., Brosse N. and Hussin M.H., 2020, Nanocellulose: From Fundamentals to Advanced Applications. *Frontiers in Chemistry*, May 2020, Volume 8, Article 392. [DOI: 10.3389/fchem.2020.00392]

Valencia Plastics, Inc., 2020, Types of Plastics Used in Pharmaceuticals. Available online at https://www.valenciaplastics.com/plastic-types-in-pharmaceuticals/

Venkatarajan S., Athijayamani A., 2020, An overview on natural cellulose fiber reinforced polymer composites. *Materials Today*: Proceedings. [DOI: 10.1016/j.matpr.2020.09.773]

Wada M. ,Heux L., Isogai A., Nishiyama Y., Chanzy H., Sugiyama J., 2001, Improved Structural Data of Cellulose IIII Prepared in Supercritical Ammonia. *Macromolecules* 2001, 34, 1237-1243 [10.1021/ma001406z CCC: $20.00]

Wang J., Gardner D.J., Stark N.M., Bousfield D.W., Tajvidi M., Cai Z., 2017, Moisture and Oxygen Barrier Properties of Cellulose Nanomaterial-Based Films. *ACS Sustainable Chem. Eng.* 2018, 6, 49−70. [DOI: 10.1021/acssuschemeng.7b03523]

Wolf C., Angellier-Coussy H., Gontard N., Doghieri F., Guillard F., 2018, How the shape offillers affects the barrier properties of polymer/non-porousparticles nanocomposites: A review. *Journal of Membrane Science* 556 (2018), 393-418. [DOI: 10.1016/j.memsci.2018.03.085]

Xu F., Wang D., 2015, Chapter 2 - Analysis of Lignocellulosic Biomass Using Infrared Methodology. Pretreatment of Biomass, *Processes and Technologies*, 2015, Pages 7-25. [DOI: 10.1016/B978-0-12-800080-9.00002-5]

Zhang J., Sun Q., Hou X., 1993, Gas Permeability in an Aromatic Polyester. *Macromolecules* 1993, 26, 7176-7181. [DOI: 10.1021/ma00078a010]

Zhu R., Yadama V., Liu H., Lin R.J.T., Harper D.P., 2017, Fabrication and characterization of

Nylon 6/cellulose nanofibrils melt-spun nanocomposite filaments. *Composites Part A: Applied Science and Manufacturing*, Volume 97, June 2017, Pages 111-119. [DOI: 10.1016/j.compositesa.2017.02.025]